NUREG/CR-6614
ORNL/SUB/97-SX754V

Feasibility of High Frequency Acoustic Imaging for Inspection of Containments

Prepared by
J.E. Bondaryk, C.N. Corrado, ORNL
V. Godino, ETC

Oak Ridge National Laboratory

Prepared for
U.S. Nuclear Regulatory Commission

DF020 | 1

NUREG/CR-6614
ORNL/SUB/97-SX754V

Feasibility of High Frequency Acoustic Imaging for Inspection of Containments

Manuscript Completed: July 1998
Date Published: August 1998

Prepared by
J.E. Bondaryk, C.N. Corrado, Oak Ridge National Laboratory
V. Godino, Engineering Technology Center

Oak Ridge National Laboratory
Operated by Lockheed Martin Energy Research Corporation
Oak Ridge, TN 37831

Subcontractor:
Engineering Technology Center (ETC)
240 Oral School Road, Suite 105
Mystic, CT 06355-1208

H.L. Graves III, NRC Project Manager

Prepared for
Division of Engineering Technology
Office of Nuclear Regulatory Research
U.S. Nuclear Regulatory Commission
Washington, DC 20555-0001
NRC Job Code J6043

For sale by the U.S. Government Printing Office
Superintendent of Documents, Mail Stop: SSOP, Washington, DC 20402-9328
ISBN 0-16-049741-8

ABSTRACT

The Nuclear Regulatory Commission has a program at the Oak Ridge National Laboratory to provide assistance in their assessment of the effects of potential degradation on the structural integrity and leaktightness of metal containment vessels and steel liners of concrete containments in nuclear power plants. One of the program objectives is to identify a technique(s) for inspection of inaccessible portions of the containment pressure boundary. Acoustic imaging has been identified as one of these potential techniques.

A numerical feasibility study investigated the use of high-frequency bistatic acoustic imaging techniques for inspection of inaccessible portions of the metallic pressure boundary of nuclear power plant containments. The range-dependent version of the OASES Code developed at the Massachusetts Institute of Technology was utilized to perform a series of numerical simulations. OASES is a well developed and extensively tested code for evaluation of the acoustic field in a system of stratified fluid and/or elastic layers. Using the code, an arbitrary number of fluid or solid elastic layers are interleaved, with the outer layers modeled as halfspaces. High frequency vibrational sources were modeled to simulate elastic waves in the steel. The received field due to an arbitrary source array can be calculated at arbitrary depth and range positions. In this numerical study, waves that reflect and scatter from surface roughness caused by modeled degradations (e.g., corrosion) are detected and used to identify and map the steel degradation. Variables in the numerical study included frequency, flaw size, interrogation distance, and sensor incident angle.

Based on these analytical simulations, it is considered unlikely that acoustic imaging technology can be used to investigate embedded steel liners of reinforced concrete containments. The thin steel liner and high signal losses to the concrete make this application difficult. Results for portions of steel containments embedded in concrete are more encouraging in that they indicate that the intrinsic backscatter from degradations representing thickness reductions from 10 to 80% the shell thickness are sufficient to permit detection. It is recommended that a controlled experimental program be conducted in which sensor levels are calibrated against degradations to determine if current sensor technology can input sufficient power into the system to provide return levels within the dynamic range of the receivers.

CONTENTS

Page

ABSTRACT iii

LIST OF FIGURES vii

LIST OF TABLES ix

EXECUTIVE SUMMARY xi

ACKNOWLEDGEMENTS xiii

1. INTRODUCTION 1

1.1 Statement of Problem and Objectives 1

1.2 Approach 1

1.3 Organization of Report 2

2. SURVEY OF PREVIOUS WORK AND AVAILABLE TECHNOLOGY 5

2.1 Previous Work 5

2.2 Available Technology 5

2.3 Conclusions 7

3. NUMERICAL MODELING – TWO-DIMENSIONAL ISSUES 9

3.1 Range-Independent OASES 9

3.2 Range-Independent Studies on Steel Containment 10

3.2.1 Scenario 10
3.2.2 Results 11
3.2.3 Conclusions 14

3.3 Range-Dependent OASES 15

3.4 Range-Dependent Studies on Steel Containment 16

3.4.1 Scenario 16

3.4.2 Results 17
3.4.3 Degradation Depth Study 20
3.4.4 Penetration Study 23
3.4.5 Source Angle Study 24
3.4.6 Conclusions 24

3.5 Range-Dependent OASES Studies on Steel-Lined Concrete Containment 26

3.5.1 Scenario 26
3.5.2 Results 26
3.5.3 Degradation Depth Study 28
3.5.4 Penetration Study 31
3.5.5 Conclusions 32

4. SYSTEM REQUIREMENTS – THREE-DIMENSIONAL ISSUES 33

4.1 Array Approach for Localization and Mapping 33

4.2 Localization and Mapping with Ultrasonic Sensors 35

4.3 Scannable Sensors 35

5. CONCLUSIONS AND RECOMMENDATIONS 37

5.1 Conclusions 37

5.2 Recommendations 38

6. REFERENCES 41

LIST OF FIGURES

Figure — Page

1-1. Breakdown of problem into two-dimensional and three-dimensional regimes. 1

2-1. Ultrasonic thickness (UT) measurement 6

2-2. Ultrasonic sensor with coupling wedge 6

2-3. Detection of a crack with ultrasonic pulse-echo technique 7

3-1. Range independent OASES simulation scenario 10

3-2. Model of steel layer surrounded by air; excited by a point source in middle of steel layer at range of 0 m for four different frequencies 12

3-3. Model of steel layer surrounded by concrete at four different frequencies 13

3-4. Model of steel layer surrounded by concrete with four different values of Gaussian roughness on bottom of steel layer 14

3-5. Simulation scenario for steel containment 16

3-6. Model of steel layer surrounded by air only 18

3-7. Model of an embedded steel containment 19

3-8 Signal level from a degradation located 5 cm from the air/concrete interface vs degradation depth and frequency. Degradation on top and bottom surfaces 20

3-9. Illustration of Rayleigh parameter, P 21

3-10. Signal level from a degradation located 5 cm from the air/concrete interface vs degradation depth and frequency. Degradation on top surface only 22

3-11. Signal level from a 4-mm-deep degradation vs distance from interface and frequency 23

3-12 Signal level from a four-mm-deep degradation 5 cm from interface vs shear angle in steel 25

3-13. Simulation scenario for steel-lined concrete containment 26

3-14. Model of an embedded steel-lined concrete containment 27

3-15. Signal level from a degradation located 5 cm from the interface vs. degradation depth and frequency 29

3-16. Model of an embedded steel-lined concrete containment 30

3-17. Signal level from a 2-mm-deep degradation vs distance from interface and frequency 31

4-1. Illustration of localization via beam steering and range gating for range determination 34

4-2. Illustration of beamforming parameters and their effect on beam shape 34

4-3. Sensor array cut from a single sensor block 36

4-4. Array spacing and beam overlap for a scannable array system 36

5-1. RD-OASES simulation scenario for additional scatterers 38

LIST OF TABLES

Table		Page
2-1.	Sensor characteristics	7
3-1.	Material properties used in OASES models	10

EXECUTIVE SUMMARY

The objective of this study is to conduct analytical simulations to investigate the feasibility of using high-frequency bistatic acoustic imaging techniques for the detection and localization of thickness reductions in the metallic pressure boundary of nuclear power plant containments. In addition, if feasible, preliminary performance requirements for a proposed high-frequency bistatic acoustic imaging system are to be identified and described. Once developed, the primary use of this technology will be to inspect inaccessible regions of the containment pressure boundary where it is embedded in concrete. While the emphasis is on free-standing steel containments, steel-lined concrete containments are also considered. An elastic layered media analysis code has been used to perform a series of numerical simulations to determine the fundamental two-dimensional propagation physics of these containment types. This includes studies on frequency, flaw size, interrogation distance, and sensor incident angle. A summary of the primary findings of this report follows:

1. Analytical simulation suggests that for the case of embedded steel containments, significant (2 mm) degradations of the containment thickness below the air/concrete interface give reasonable intrinsic backscatter signal levels of approximately –15 dB. This yields signals that are 10-15 dB above the expected effective noise level due to surface imperfections. For degradation representing thickness reductions from 10% to 80% of shell thickness, the variation of the backscatter with depth of the degradation is small, only 10 dB, but measurable. The embedding concrete introduces large losses, 3-4 dB two-way loss per cm of concrete, and will limit penetration capability. Backscatter strength is not very sensitive to frequency or angle of the transducer (<5 dB) for the sharp-edge degradations examined here. It is therefore probable that, given enough sensor input power, acoustic imaging technology can be applied to this scenario.
2. Analytical simulation suggests that for the case of embedded steel-lined concrete containments, the thin steel layer and additional concrete backing contribute to give unacceptable loss of signal to the concrete. Approximately 100 dB of signal loss is incurred for a small degradation close to the interface. Due to this loss, it is highly unlikely that acoustic imaging technology can be applied to this scenario.
3. A limited sensor survey was made to determine the characteristics of currently available ultrasonic sensor technology. The sensors of interest are intended to excite shear waves in the steel and consist of a piezo element and coupling wedge. Ultrasonic transducers used in current applications are uncalibrated devices. This means that *absolute* vibration levels in the containment scenario cannot be accurately predicted and the suitability of these devices for this application cannot be assessed. Calibration of available sensors is the highest priority recommendation for future work.
4. Currently available piezo sensors cannot be used in array configurations to interrogate a large area due to their intrinsic narrow beampattern, which does not allow steering. This limits these sensors to spot detection and mapping scenarios, where degradation is already suspected. For wide area surveys, the use of scannable sensors appears to be applicable, but they will require development in conjunction with industry, such as has been done for medical ultrasound. The sensors would be manufactured by bonding many signal wires to a

solid piezoelectric block on a substrate and then cutting the piezo into individual sensors, leaving a line array of sensors in the substrate

ACKNOWLEDGMENTS

The financial and technical support of the Oak Ridge National Laboratory and the U. S. Nuclear Regulatory Commission are greatly appreciated. We would also like to thank Mr. R. F. Sammataro for his assistance in providing information related to nuclear power plant containments.

1. INTRODUCTION

1.1 Statement of Problem and Objectives

An area of concern in nuclear power plants is the potential for moisture-induced, thickness degradation of the embedded metallic pressure boundary adjacent to and below the interface where it enters the concrete. This is an area that cannot be examined by traditional ultrasonic thickness (UT) testing due to the inaccessibility imposed by the concrete. The overall objective of this activity is to demonstrate the feasibility of using high frequency bistatic acoustic imaging techniques for the detection, localization, and mapping of thickness reductions in the metallic pressure boundary of nuclear power plant containments. The primary use of this technology will be to inspect inaccessible regions of the containment where it is either embedded in concrete or adjacent to floors or equipment. While the emphasis is on free-standing steel containments, steel-lined concrete containments are also considered.

1.2 Approach

The overall problem breaks down into two broad and fairly independent sub-problems, which are shown in Fig. 1-1 for the steel containment scenario. Each of these problems is treated separately in this document, two-dimensional issues are treated in Chapter 3 and three-dimensional issues are treated in Chapter 4.

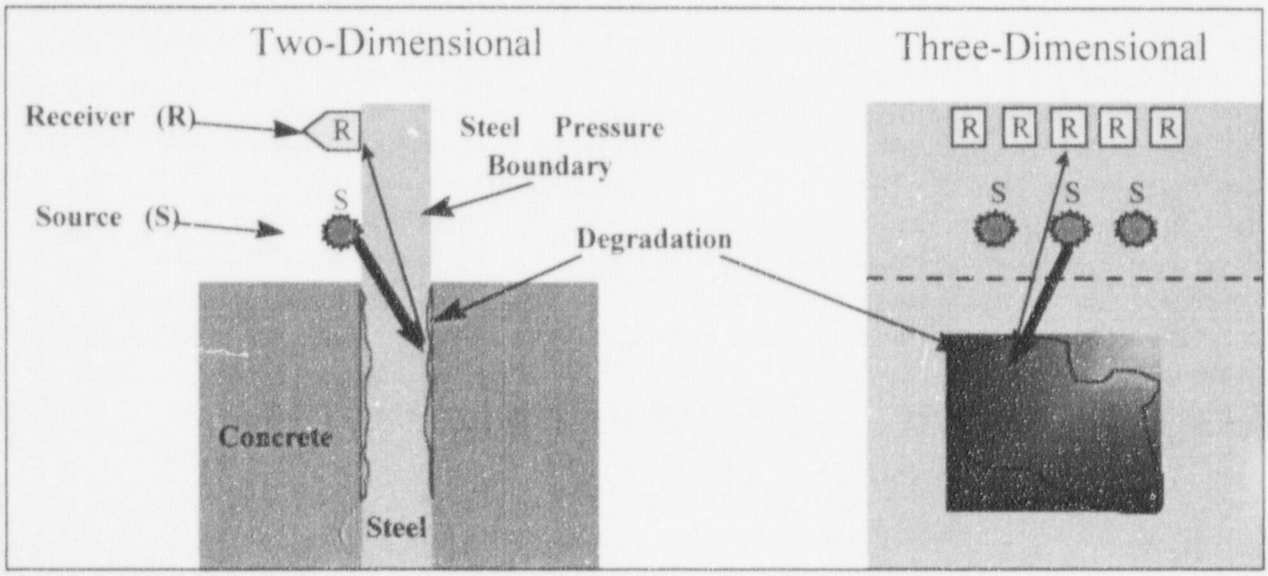

Fig. 1-1. Breakdown of problem into two-dimensional and three-dimensional regimes. Left of figure shows multi-layered system with degradation layer between steel and concrete. Right of figure is a side view of left and shows a finite patch of degradation.

The left of this figure shows an end-on, two-dimensional view of the problem. A steel layer extends up and down from an interface. Above the interface, the steel is surrounded by air. Below the interface, the steel is surrounded by concrete. The area of interest is confined to the region up to about 30.5 mm below this interface. Here, it is believed that water intrusion due to breakdown of a moisture barrier has the potential to cause corrosion of the steel layer surface as indicated in the figure. This corrosion causes thinning and pitting of the steel layer. It is believed that these discontinuities in the steel layer surface could be detected by acoustic imaging methods. As shown in the figure, a source, denoted by "S", would inject sound into the steel layer. The sound would travel down into the degraded region and bounce off any surface discontinuities. This scatter would propagate back up the steel layer and be detected by a receiver, labeled "R." This two-dimensional problem provides a set of fundamental constraints. Here, the physics involve propagation of high frequency waves inside a layered system. This geometry and the material properties of the various media determine how waves will travel in the system. Modeling of this part of the problem will determine which frequency ranges and wavetypes will be best for propagation into the area of interest. In this study, numerical modeling is used to calculate the field in this layered system to determine backscattered pressure levels due to the source waves bouncing off degradation having various depths and distances from the interface. The OASES code, developed at the Massachusetts Institute of Technology (MIT), is used in this study to model the acoustic field in the system. Further details are given in Chapter 3. The bulk of this report is devoted to the two-dimensional issues associated with this problem as they are the most important determinants of system performance.

The right side of Fig. 1-1 illustrates the three-dimensional issues associated with this problem. This is a side view of the left hand figure, with the interface denoted by the dotted line. It is believed that the degradation will have some finite extent over the surface of the containment. A line of sources and receivers is shown interrogating the degradation. An array of this configuration can form beams of sound and sweep out an angular region on the containment. In a similar fashion, the pulse character of the signal will allow a range gating of the signal. Combined, these will allow a system to draw a map of the containment surface indicating the depth of the degradation in each spatial bin. The frequencies determined by the two-dimensional studies and the sensor characteristics will determine the size and spacing of these bins. The penetration and scanning capability in turn will determine the overall operation of the system. Once frequencies and wavetypes are set by the two-dimensional problem, all that remains is determining the appropriate sensors and sensor array geometries to give adequate scanning extent and resolution. This part of the problem will be addressed analytically in Chapter 4, given the sensor characteristics and the results of the numerical studies.

1.3 Organization of Report

This chapter of the report has detailed the objectives of this study and outlined the proposed approach to provide a solution to the inspection of containment degradation in inaccessible areas. Chapter 2 summarizes several previous efforts done in this area and identifies available acoustic sensor technology. It will be seen that sensors in current typical applications are not adequately calibrated to allow prediction of their suitability for this application. The lessons learned and sensor parameters derived from this information are used as a guide in the numeric models of Chapter 3. Here a layered media code (OASES) is used to determine the

fundamental two-dimensional propagation physics of the scenario under investigation. This includes studies on frequency, flaw size, interrogation distance, and sensor incident angle. Results are presented for the case of a steel containment and a steel-lined concrete containment. Here, it is shown that it is probable for high frequency acoustic imaging to be applied successfully to the steel containment scenario, but not for the steel-lined concrete containment. Chapter 4 provides preliminary design and specification of an inspection system, based on some identified sponsor requirements and guided by the results of the numeric study of Chapter 3. Contained in Chapter 5 are study conclusions and recommendations for future work. Finally, Chapter 6 provides reference sources used in the study.

2. SURVEY OF PREVIOUS WORK AND AVAILABLE TECHNOLOGY

2.1 Previous Work

A limited literature survey and the references for these papers shows that the current ultrasonic scattering research is highly theoretical and mostly analytic [1-6]. Analytically predicting scatter from surface degradations for this scenario could represent a lengthy research topic. Much ultrasonic experimental work has been done for what amounts to far less challenging scenarios (e.g., detection of accessible flaws in airframes). Discussions with nondestructive examination (NDE) experts indicate that researchers in the field are just now becoming interested in problems similar to the embedded containment problem, mostly for detecting flaws in inaccessible areas of airframes [7]. Due to the high complexity of the problem, and lack of practical information in the literature, it was decided that a numerical model would be the only possible approach that would fit within the time and budget constraints of this study.

By far the most interesting study example of this kind of work is found in Section 3.4 of Ref [1]. Here, qualitative measurements were made on degraded test blocks and containments using available sensor systems. The study demonstrates that some 2-mm-deep degradations can be detected with moderate to high confidence using a 2 MHz, 45-degree ultrasonic sensor, depending on the degree of pitting in the degradation. Conclusions in the reference are slightly pessimistic, since the system used did not operate over a very wide dynamic range. The study did *not* include examples where the test article was embedded in concrete, and thus conclusions can *not* be applied directly to the present scenario, as will be shown in Chapter 3 of the present study. While too qualitative and incomplete for specific conclusions, observations in the reference are highly consistent with lessons learned from the OASES simulations in Chapter 3 of this study. We, therefore, have confidence in our tools.

2.2 Available Technology

A limited sensor survey was made to determine the characteristics of currently available ultrasonic sensor technology [6]. Most UT systems, and in fact most ultrasonic applications, operate in a compressional pulse-echo mode as illustrated in Fig. 2-1. A voltage is applied across a piezo-ceramic element. The element responds by creating a displacement proportional to this voltage. A compressional wave is thus introduced into the medium under test. The wave reflects from the far surface and sends a compressional wave back towards the sensor. The sensor also acts as a receiver and picks up this return pulse. A system such as this where the source and receiver are at the same location is called a monostatic system (a system where the source and receiver are not co-located is known as a bistatic system). The time it takes for the pulse to make a round trip, $2T$, is measured. The compressional sound speed of the material, C, must be known. The thickness of the material, H, is thus given by $H = T^*C$. This technique is used where the sensor can access directly the area of interest. Such is not the case in the problem under consideration in this study.

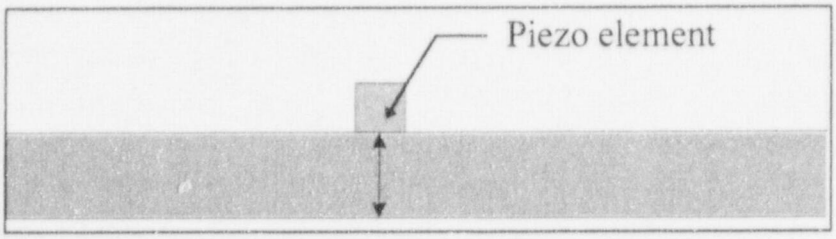

Fig. 2-1. Ultrasonic thickness (UT) measurement. The layer thickness is equal to the time for the pulse to propagate through the thickness multiplied by the soundspeed of the material.

The sensors of interest for the embedded containment scenario are those capable of exciting waves which propagate laterally in the layer as illustrated in Fig. 2-2.

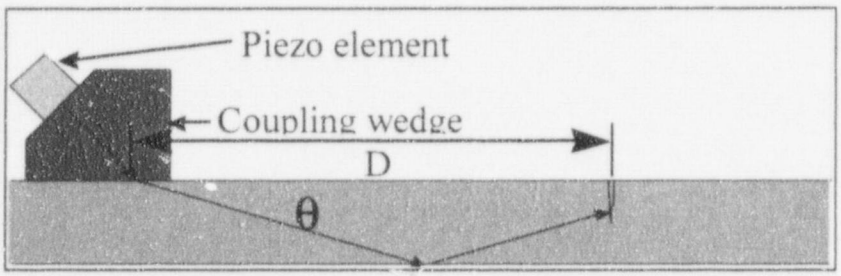

Fig. 2-2. Ultrasonic sensor with coupling wedge. Vibrational energy propagates laterally through layer. Imperfections in material reflect energy back to piezo element.

The wave must propagate sideways, guided in the layer, to the region where the steel is surrounded by concrete, and return. In order to do this, the piezo element is mounted at an angle to the test medium via a coupling wedge material, usually plastic. The material properties and angle of the wedge are carefully chosen. The compressional wave excited in the wedge is coupled to the shear wave in the steel, in this case at an angle of θ, via trace matching. This is also known as Snell's law, which states that the sine of the angle in the wedge over the compressional wavespeed must equal the sine of the angle in the steel over the shear wavespeed:

$$\frac{Sin\theta_w}{c_w} = \frac{Sin\theta_s}{c_s}$$

The shear wave in the steel is used rather than the compressional wave, as it is more strongly coupled at such angles. Flaw detection is done by looking for pulse echo returns from cracks as illustrated in Fig. 2-3. Unfortunately, only the qualitative presence of additional pulses and the time between pulses is typically used to determine the presence of flaws. Sensors by and large are completely uncalibrated. Manufacturers do not know what vibrational levels are injected into the media by their transducers, nor do they know what returned levels are necessary for

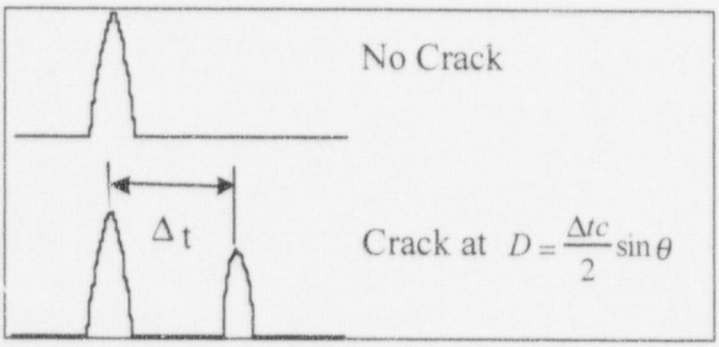

Fig. 2-3. Detection of a crack with ultrasonic pulse-echo technique. The crack causes echo of initial pulse which arrives at a time proportional to its distance from the piezo element.

guaranteed detection by their receivers. This will be a major limitation in this feasibility study. Poor sensor characterization means that absolute vibration levels in the containment scenario cannot be accurately predicted. Better calibration of currently available sensors is one of the important recommendations for future work.

For the purposes of using realistic sensor characteristics in the numerical work of Chapter 3, a survey of sensors was made and typical values for important parameters were identified and are listed in Table 2-1.

Table 2-1. Sensor characteristics.

Frequencies	0.5, 1.0, 2.25, 3.5, 5.0 MHz
Q = Δf/fc	0.6
Size	0.25", 0.5", 1.0" in diameter
Shear Angles in Steel	30, 45, 60, 70 degrees
Typical Cost	pulser/receiver - $7K, sensors - $400

In addition to sensor manufactures, service companies that make commercial UT measurements were also identified and may be useful if extensive field testing of systems is required.

2.3 Conclusions

The characteristics of current sensor technology are inadequately specified and calibrated to determine their applicability to the problem of current interest. However, the frequency ranges, sizes, and orientations of available sensors provide an important guide for modeling. Previous efforts to detect surface degradations have met with moderate success, which provides confidence in the method.

3. NUMERICAL MODELING – TWO-DIMENSIONAL ISSUES

The bulk of this report deals with estimation of the field in a two-dimensional containment scenario via numerical modeling. The left side of Fig. 1-1 shows the two-dimensional scenario under consideration. Here the medium and field are assumed to be infinitely homogeneous in the plane out of the paper. Thus, any slice, as shown, is representative of the entire problem. This is a reasonable approximation that allows the basic physics of the layered propagation problem to be determined. Due to the high complexity of the embedded containment problem, analytic approaches to this problem would have been prohibitively time consuming and costly considering constraints of this study. It was decided that numerical modeling was the only practical approach to calculation of the scattered field in the two-dimensional scenario. The OASES code was selected as a state-of-the-art computational engine for calculation of the acoustic field in stratified problems. A range-independent and range-dependent version of the code were used in turn to examine the containment scenarios.

3.1 Range-Independent OASES

ETC obtained a range-independent version of the OASES code (RI-OASES) [8,9] from the website [10] of Prof. Henrik Schmidt of the MIT Department of Ocean Engineering. This is a well developed and extensively tested code for the evaluation of the acoustic field in a system of stratified fluid and/or elastic layers. The propagation scenario must be horizontally layered with the material parameters of each layer fully specified in sound speed, density, and absorption. An arbitrary number of fluid or solid elastic layers can be interleaved, though the outer layers are modeled as halfspaces. The received field due to an arbitrary source array can be calculated at arbitrary depth and range positions. The response is calculated for a single frequency via an exact fully elastic calculation by wavenumber integration, no approximations other than the usual computer precision issues exist. The algorithm is unconditionally numerically stable. While single frequency calculations were sufficient for the purposes of this project, the code can also loop over frequency and Fourier transform the results into the time domain to form a complete pulse simulation. RI-OASES was compiled, installed, and tested on a Pentium PC running the Linux 2.0 operating system. Benchmarks indicate that the program operates consistently with manual specifications.

Table 3.1 shows the material properties used in all RI-OASES numerical models as well as all RD-OASES numerical models run for the purposes of this report. These are properties for "average" materials, obtained from standard sources [11]. Deviations from these values on the order of 10% can be expected for specific materials.

Table 3-1. Material properties used in OASES models.

Material	Modulus E (GPa)	Shear Modulus G (GPa)	Density ρ (kg/m^3)	Comp. speed c_p (m/s)	Shear speed c_s (m/s)	Lamb speed c_r (m/s)	Loss Factor η	Poisson ratio ν
Steel	200	77	7850	5048	3132	2896	1e-4	0.28
Concrete	24	9	2569	3056	1872	1747	2e-2	0.34
Air			1.2	345			3.5e-3	

3.2 Range-Independent OASES Studies on Steel Containment

3.2.1 Scenario

A preliminary and approximate model of the containment scenario was created as illustrated in Fig. 3-1. This model is representative of the portion of the problem either above or below the interface but does not represent the interface itself. The problem, relative to Fig. 1-1, has been rotated 90 degrees to allow the layer structure to be modeled exactly by RI-OASES. A nominal 25-mm-thick steel layer represents the containment. The steel is surrounded by concrete halfspaces (or air halfspaces for initial comparison purposes) A nominal 25-mm-long source array represents the ultrasonic sensor. Several explosive pressure point sources are spaced to avoid aliasing at the given frequency. The array is normalized to 1 Pa at 1 m in a far-field

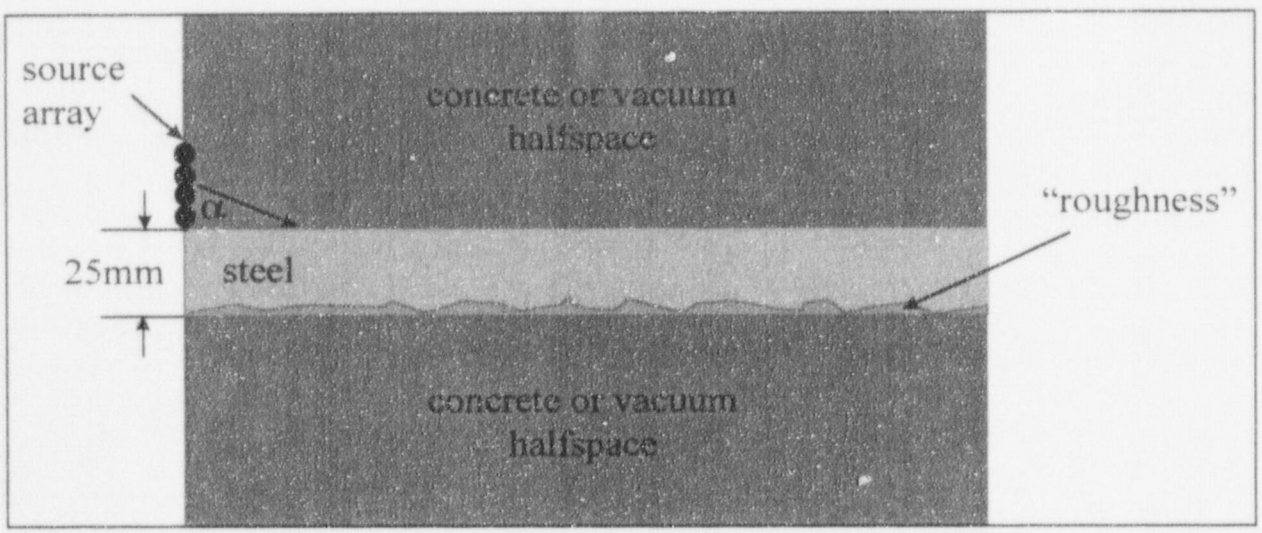

Fig. 3-1. Range independent OASES simulation scenario. 25-mm steel layer surrounded by concrete or vacuum halfspaces. Roughness on bottom surface of steel represents surface degradation.

sense. The array is steered down at an angle to couple to a particular shear wave angle in the steel. The model was run for angles and frequencies of currently available commercial sensors noted in Table 2-1. The model assumes a plane geometry (i.e., all layers extend homogeneously and infinitely out of plane). Normal stress was calculated over a grid at a spacing of 1 cm in range and depth. The field is calculated to a range extending from the source at 0 m to a distance of 1 m. The field is calculated to a depth extending from 25 mm above to 25 mm below the steel layer. (Of course, the layers beyond these calculated depths and ranges extend to infinity in the model.)

Degradation of the steel layer is represented by spatially uncorrelated surface roughness on the bottom surface of the steel layer. The roughness extends infinitely over the entire bottom surface due to the constraints of the model. The root-mean-square (RMS) height of this roughness was used to parameterize the degradation. It was hoped that this simple model would be sufficient to understand the physics of the scenario. However, after extensive manipulation of this model, it became clear that this range independent version of the scenario was inadequate to capture the important processes of propagation. In particular, the surface roughness is a poor representation of degradation, which is the way it is implemented in this code. It will be shown below that range dependence is required to fully understand this problem.

3.2.2 Results

It is believed that the presence of the concrete should have a very significant effect on the problem. It is therefore initially of interest to look at the results of the propagation without the concrete and without roughness. Figure 3-2 shows the results of the simulation of a steel layer, surrounded by vacuum, excited by a point source in the middle of the steel at four different source frequencies. The plots show the normal stress in dB as a function of depth in centimeters and range in meters. The acoustic field is contained entirely in the duct formed by the steel layer. The structure in the field is due to the cross thickness modes which exist in the plate. More modes cut on as the frequency increases causing a more complex structure to the field. Note that attenuation due to absorption by the steel layer is fairly low, only 5-20 dB over 1 m. In this case, energy propagates essentially unimpeded along the steel layer.

To explore the influence of the concrete, the same parameters were run for a model where the material above and below the steel layer was concrete. This time the source is a 25-mm-long array on top of the steel whose elements are phased to excite a 45-degree shear wave in the steel. The results for this model are shown in Fig. 3-3. This time there is significant loss of energy to the concrete, on the order of 70 dB over 1m. This loss can be seen as the high field levels above and below the steel layer in all plots. The mechanism here is phase speed matching of the shear wave in the steel into compressional waves in the concrete. Since energy leaks off, via Snell's law, into waves in the concrete, it is the wavespeed of the concrete that is important and not its intrinsic absorption. This is a significant loss mechanism, which will ultimately limit the penetration ability of any practical system.

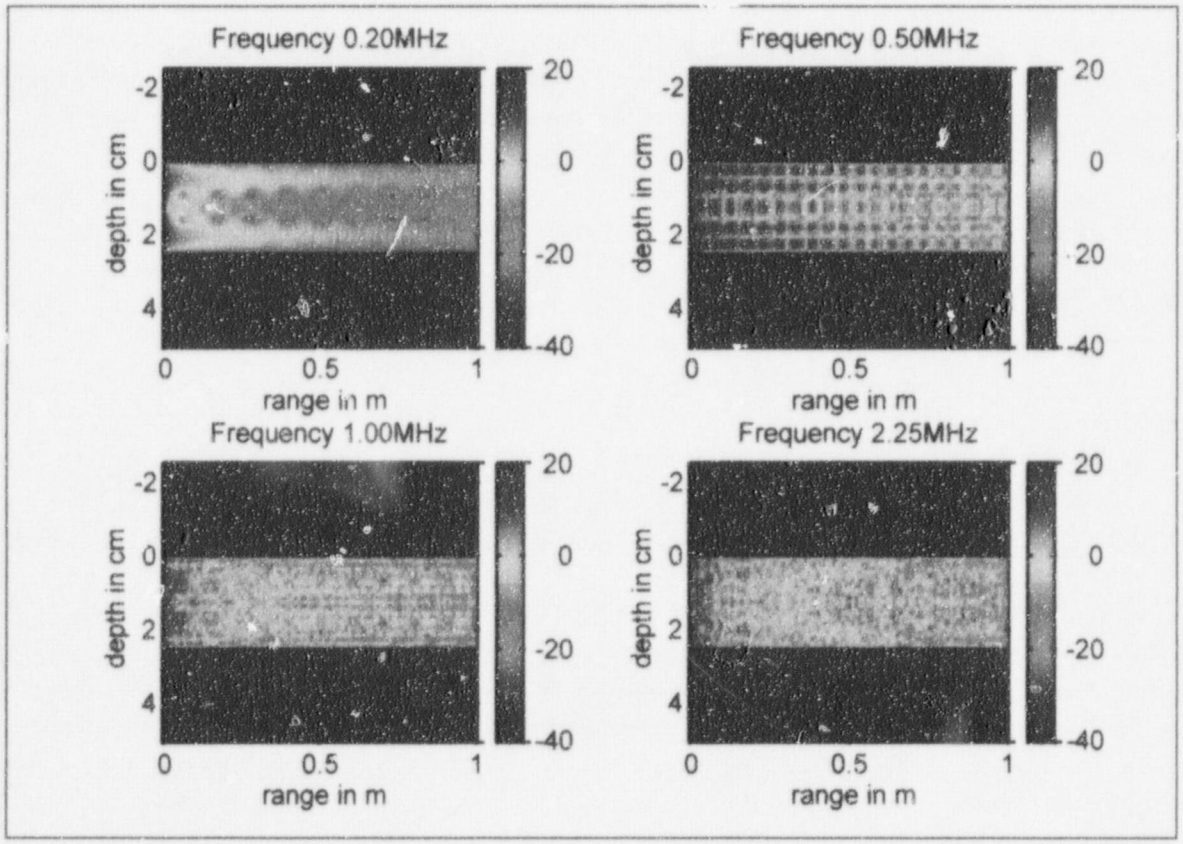

Fig. 3-2. Model of steel layer surrounded by air; excited by a point source in middle of steel layer at range of 0 m for four different frequencies. Colors represent normal stress in dB. The structure in the field is due to the cross thickness modes which exist in the plate. More modes cut on as the frequency increases causing a more complex structure in the field. Note that attenuation due to absorption by the steel layer is fairly low; only 5 - 20 dB over 1 m.

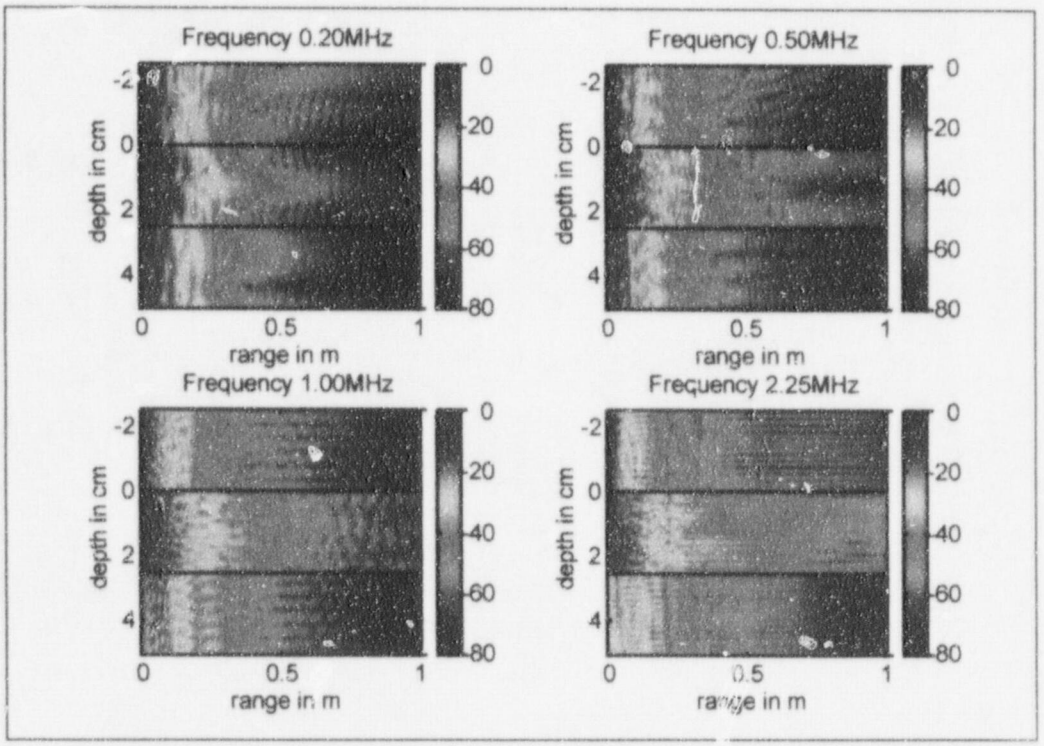

Fig. 3-3. Model of steel layer surrounded by concrete at four different frequencies. Source is a 25-mm-long array that excites a 45-degree shear wave at selected frequencies in steel, located at 0 m range above top surface. Colors represent normal stress in dB. Note that there is significant loss of energy to the concrete; over 70 dB over 1 m as compared to 5 - 20 dB for steel surrounded by air. This is a significant loss, which will limit the capability to detect corrosion of the steel much below the concrete surface.

Finally, the effect of roughness was tested for the scenario with a steel layer between two concrete halfspaces. An uncorrelated Gaussian surface roughness was placed on the bottom interface. This roughness extended infinitely along the plate due to the constraints of the model. The RMS height of the roughness was varied from 0 to 8 mm, which represents up to a 30% thickness degradation. Figure 3-4 shows the results of this model for a 25-mm source array at a frequency of 0.5 MHz.

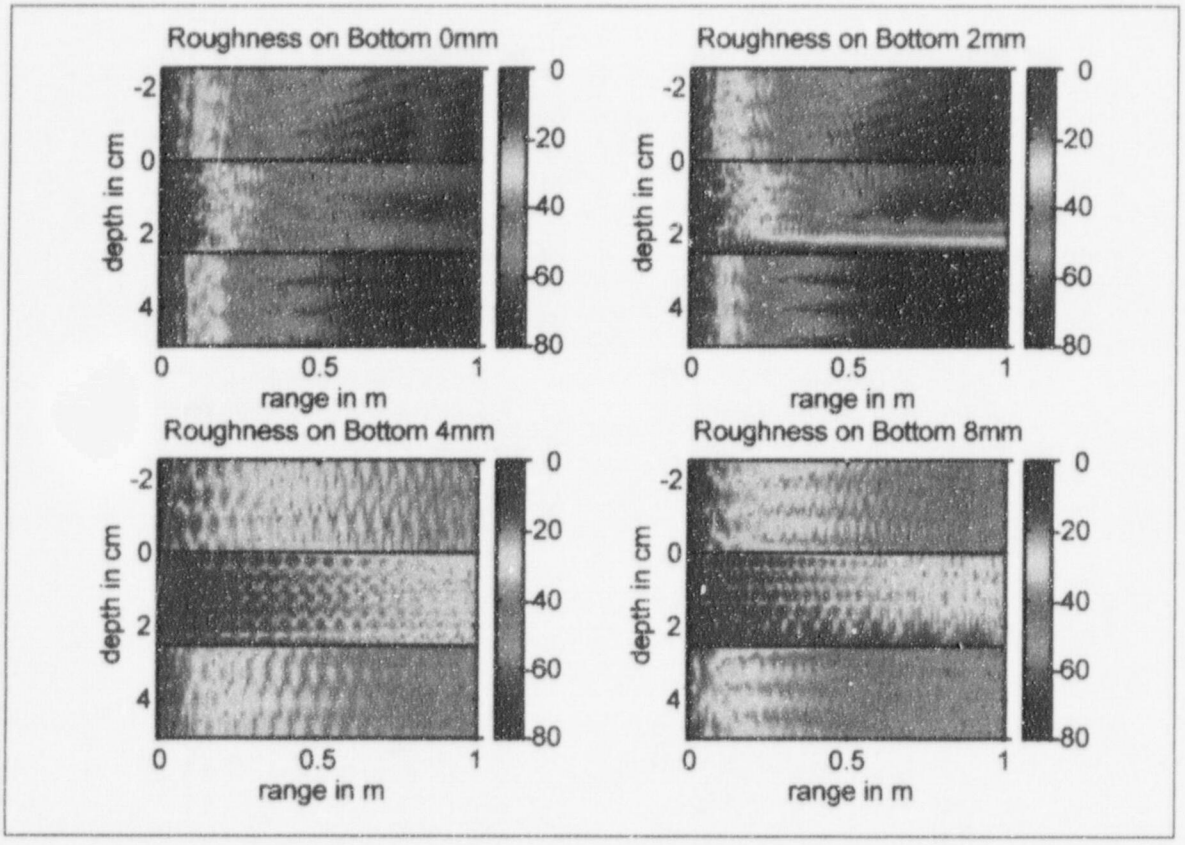

Fig. 3-4. Model of steel layer surrounded by concrete with four different values of Gaussian roughness on bottom of steel layer. Source is a 0.5 MHz, 25-mm long array that excites a 45-degree shear wave, located at 0 m range above top surface. Colors represent normal stress in dB. An unphysical amount of energy is present in the roughness layer. Also, the model becomes unstable as the roughness height approaches the layer thickness. This model of the degradation cannot be used for this scenario.

There are several problems with this roughness representation. First, the acoustic field is undefined within the roughness layer. The levels on the interface are essentially meaningless. More importantly, high roughness, on the order of the layer size, causes unphysical results because the underlying assumptions are violated. This is seen as an increase in the total energy in the field as roughness is increased. It is not physically possible for more energy to exist in the system due to the addition of this passive element. Finally, RI-OASES models the effect of roughness simply as an attenuation of the forward propagating wave. No backscattered wave is generated by the roughness. Thus, no model of this type will be able to generated a "return" from the rough surface. The model is simply inappropriate for the application.

3.2.3 Conclusions

The Range-Independent OASES studies confirm the ability of this code to model the basic scenario. Clear modal structural dependence on frequency was seen. This was accompanied by the higher injection of energy into the steel layer. Also present was the

attenuation of the field increasing slightly with frequency. Finally, trace matching to propagating waves in the concrete was identified as the primary mechanism for the high loss of energy from the steel layer.

Enlightening as these initial studies were, it also became quite apparent that RI-OASES is insufficiently suited to model this problem. In particular, the surface roughness approach to modeling of thickness degradations is not applicable with this code. Not only is the field undefined within roughness, but roughness on the order of the layer size causes instability in computation. However, the basic flaw in this approach is the lack of backscatter in the OASES roughness model. Based on these RI-OASES studies, it was decided to abandon the surface roughness modeling approach. By moving to Range Dependent-OASES, the full interface scenario could be modeled and a new degradation approach, based on discrete degradation patches, could be applied.

3.3 Range-Dependent OASES

In order to circumvent the modeling limitations introduced by the Range- Independent version of OASES, the Range-Dependent version of the OASES code was employed. This allowed modeling of the full scenario, which includes the air/concrete interface, a finite length source, and discrete degradation patches.

The Range-Dependent version of the OASES code (RD-OASES) from MIT [8-10] was selected as a state-of-the-art computational engine for calculation of the acoustic field in stratified problems. This is a well-developed and extensively validated code for the evaluation of the acoustic field in a system of stratified fluid and/or elastic layers. The problem is broken up into vertical sectors. Each sector must be horizontally layered with the material parameters of each layer fully specified in sound speed, density, and absorption. An arbitrary number of fluid or solid elastic layers can be interleaved, though the outer layers are modeled as halfspaces. The received field due to an arbitrary source array can be calculated at arbitrary depth and range positions. The response is calculated for a single frequency in each sector via an exact fully-elastic calculation by wavenumber integration, no approximations other than the usual computer precision issues exist. The algorithm is unconditionally numerically stable. The field in one sector is propagated to the next sector by a virtual array of sources located on the sector boundary. A single scatter model is used (i.e. the field is calculated once forward through the sectors and then once backward). While single frequency calculations were sufficient for the purposes of this project, the code can also loop over frequency and Fourier transform the results into the time domain to form a complete pulse simulation. RD-OASES was compiled, installed, and tested on a Pentium PC running the Linux 2.0 operating system. Benchmarks indicate the program operates consistently with manual specifications.

3.4 Range-Dependent OASES Studies on Steel Containment

3.4.1 Scenario

The two-dimensional numerical model for the embedded steel containment scenario is shown in Fig. 3-5. The problem relative to Fig. 1-1 has been rotated 90 degrees to allow the layered structure to be modeled exactly by RD-OASES. A nominal 25-mm-thick steel layer represents the containment. The steel is surrounded by air halfspaces above the midpoint of the simulation and by concrete halfspaces (or air halfspaces for initial comparison purposes) below the midpoint. Degradation of this steel layer is represented by a 10-cm-long notch cut from both surfaces. The thickness of this degradation, T, and its distance from the interface, dx, are parameters of the simulation. A nominal 25-mm-long source array in a "wedge" material represents the ultrasonic sensor. The wedge material is modeled as a fluid and thus supports only compressional waves. Several explosive pressure point sources are spaced to avoid aliasing at the given frequency. The array is normalized to 1 Pa at 1 m in a far-field sense. The array is steered down at an angle to couple to a particular shear wave angle in the steel. The model was

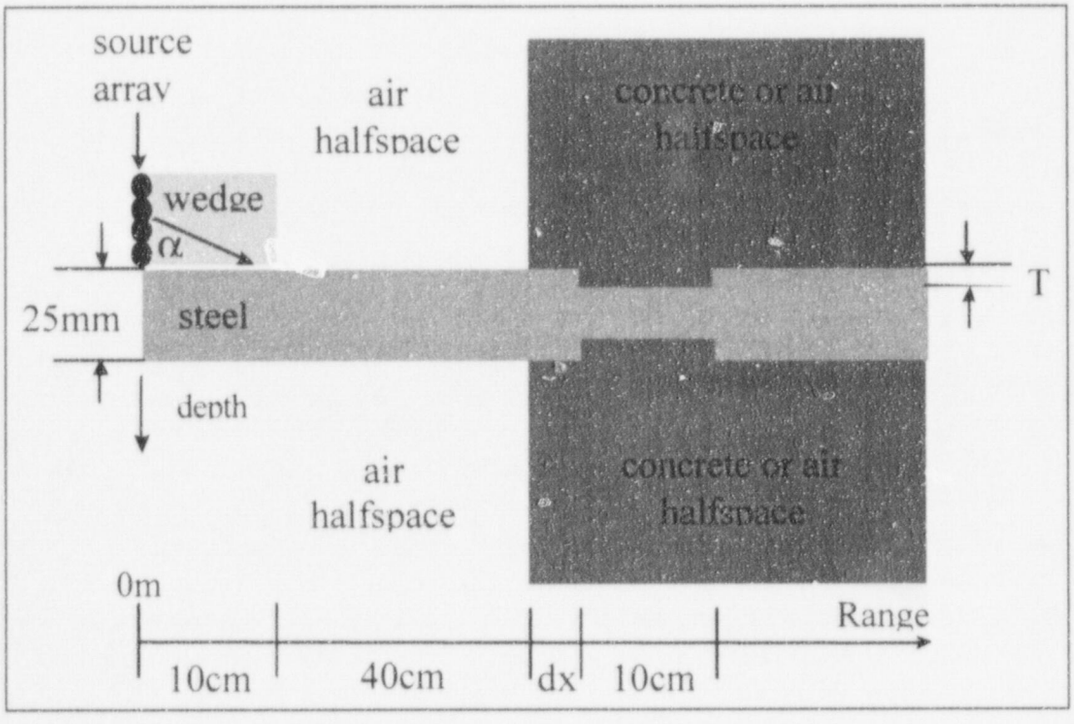

Fig. 3-5. Simulation scenario for steel containment. 25-mm steel layer surrounded by air halfspaces on the left and by concrete or air halfspaces on the right. Degradation is modeled by a two-sided 10-cm notch cut from the steel layer and filled with concrete. The thickness of the layer, T, and its distance from the interface, dx, are parameters of the simulation.

run for angles and frequencies of currently available commercial sensors in Table 2-1. The model assumes a plane geometry (i.e. all layers extend homogeneously and infinitely out of plane). Normal stress was calculated over a grid at a spacing of 1 cm in range and depth. The calculated range extended from the source at 0 m to a distance of 1 m. The calculated depth extended 25 mm above and below the steel layer. (Of course, the layers and sectors beyond these calculated ranges extend to infinity in the model.) The code naturally separates the forward-scattered field from the back-scattered field.

3.4.2 Results

The earlier range-independent studies demonstrated that the presence of the concrete should have a very significant effect on the problem. It is therefore of interest to look at the results of the propagation without the concrete.

Figure 3-6 shows the results of the simulation for a 0.5 MHz source which excites a 45-degree shear wave in the steel. The steel is surrounded by air only. There is degradation on both sides of the steel, T = 4 mm, located at R = 0.55 m (i.e., 5 cm to the right of where the interface will be in the full scenario shown in Figure 3-5). The top plot shows the normal stress in dB as a function of range and depth for the forward-propagating field. Note that attenuation due to absorption by the steel layer is fairly low. The middle plot shows the same for the backward-propagating field. Note here that the degradation has caused significant reflection of energy. The bottom plot shows line plots of the forward- (blue) and backward- (red) propagating field at the top of the steel layer (i.e., at D = 0). To make quantitative comparisons in all cases, a common measure, called the "signal level," was computed as follows. The blue curve, representing forward-propagating field values at the top surface, was averaged over the range 10 to 50 cm, as indicated in Fig. 3-6. The same average was made for the red curve, representing the backward-propagating field. The forward average was then subtracted from the backward average to give the signal level. This number should represent the backscattered level seen by the sensor, located at 0.3 m, due to a unit normal stress input at that position. For this scenario, the degradation gives a signal level, SL = -17 dB. This includes the scattering strength of the degradation and the attenuation in the steel. The modal character of the field should be averaged out here. This return is a significant and easily measurable value.

To explore the influence of the concrete, the same parameters were run for a model where the material to the right of the interface was concrete. The results for this model are shown in the exact same format in Fig. 3-7. Again the degradation is a 4-mm, two-sided notch located 5 cm to the right of the interface. This time there is significant loss of energy to the concrete. This can be seen as the high field levels above and below the steel layer to the right of the interface in both the forward and backscatter plots. The mechanism here is phase-speed matching, shear waves in the steel leak off via Snell's law into compressional waves in the concrete. Notice in the bottom curve how the forward-scatter field decreases at a higher slope to the right of the interface than it does to the left. The signal level is now, SL = -37 dB. An additional 20 dB of energy, normally seen by the sensor, has been lost due to leakage into the concrete. This is a significant loss mechanism, which will ultimately limit the penetration ability of any practical system.

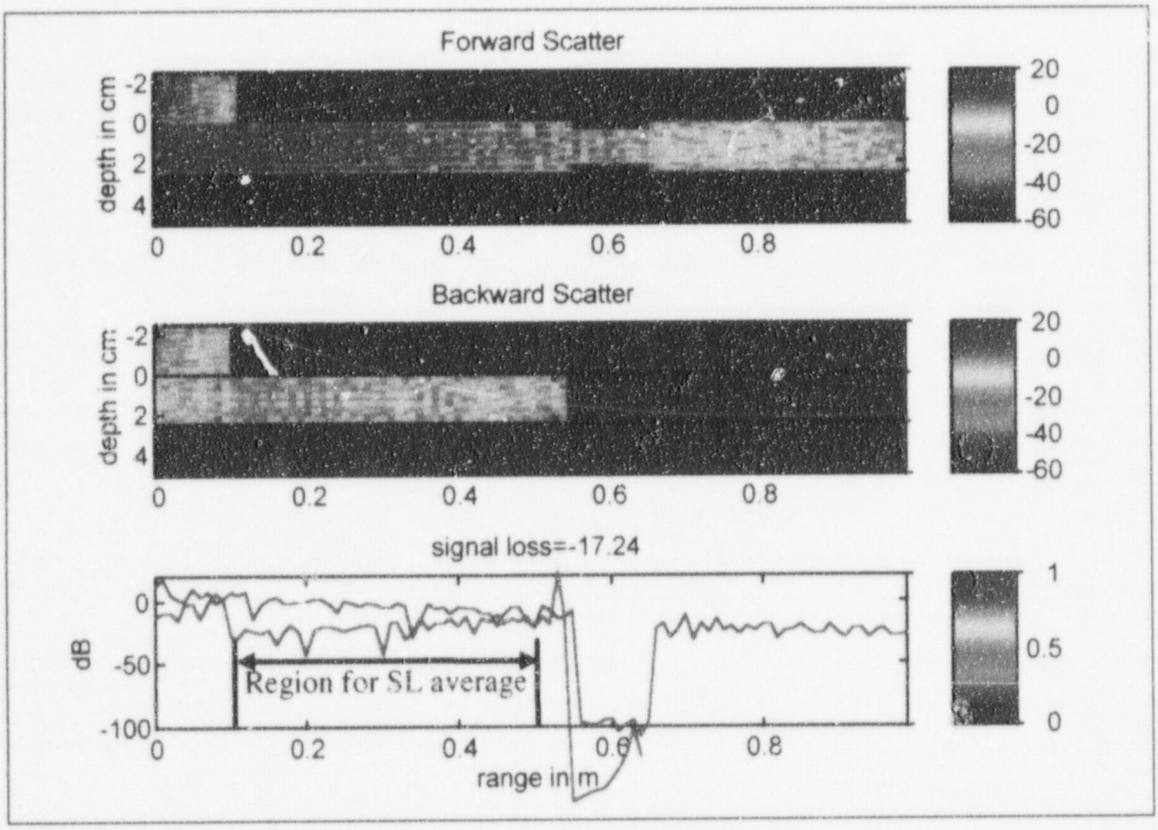

Fig. 3-6. Model of steel layer surrounded by air only. The source is a 0.5 MHz, 25-mm long array which excites a 45-degree shear wave in steel, located at 0m range. The degradation is modeled as a two-sided, 4-mm-deep notch, 10-cm long, starting at 0.55 m. The top plot represents the forward-propagating energy as a function of distance and depth, and the middle plot represents the backward-propagating energy. Colors represent normal stress in dB. The bottom plot shows the forward-propagating amplitude measured at the top surface in blue and the backward in red. Signal loss is an average value of the difference of these two over the range 10 to 50 cm. This shows that without concrete the energy reflected from the notch is about 13 % of the energy input.

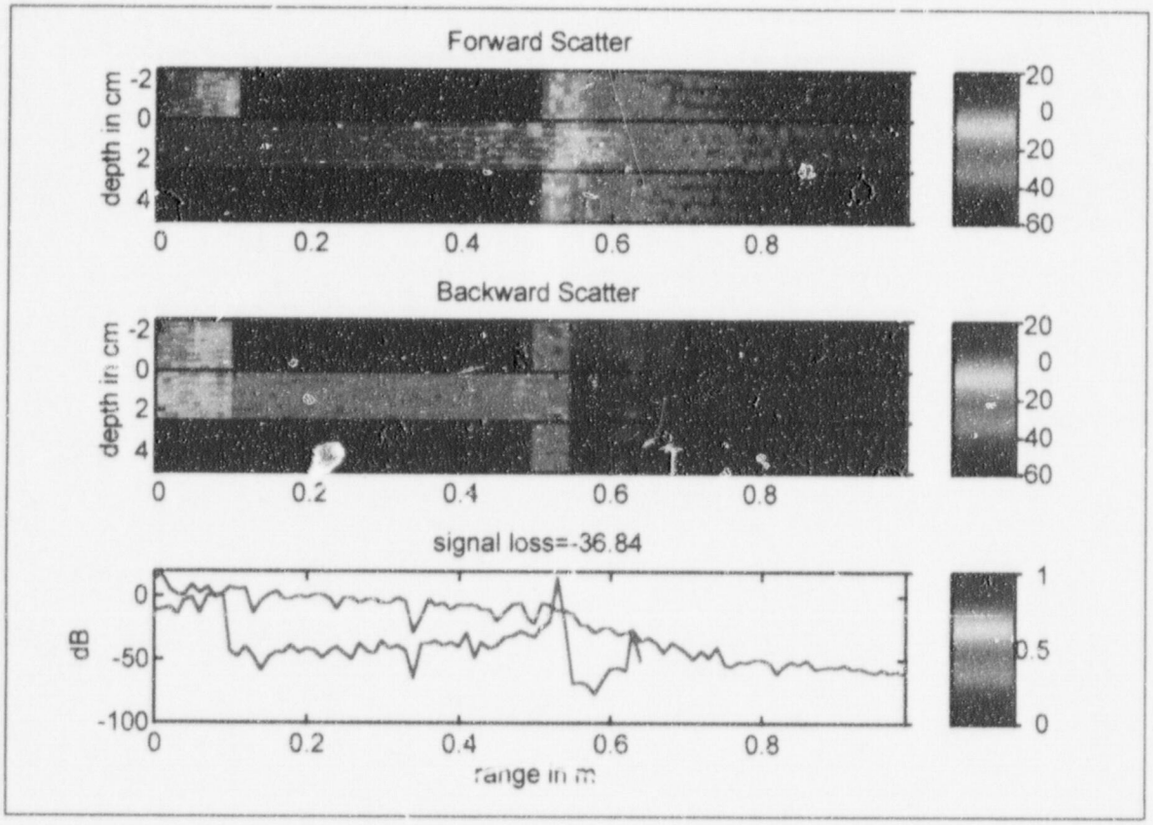

Fig. 3-7. Model of an embedded steel containment. The source is a 0.5 MHz, 25–mm-long array which excites a 45-degree shear wave in steel, located at 0 m range. The degradation is modeled as a two-sided, 4-mm-deep notch, 10-cm long, starting at 0.55 m. The top plot represents the forward-propagating energy as a function of distance and depth, and the middle plot represents the backward-propagating energy. Colors represent normal stress in dB. The bottom plot shows the forward-propagating amplitude measured at the top surface in blue and the backward in red. Signal loss is an average value of the difference of these two over the range 10 to 50 cm. This shows that the presence of the concrete has introduced an addition 20 dB (factor of 10) decrease in the energy reflected from the notch.

3.4.3 Degradation Depth Study

In order to determine the dependence of the field on frequency and depth of the degradation, the model of Fig. 3-5 was run parametrically. Frequencies of 0.1, 0.2, 0.5 and 1 MHz were run for a two-sided degradation whose depths ranged from 0.5 to 10 mm, incremented by 0.5 mm. Figure 3-8 shows a plot of signal level in dB versus degradation depth in millimeters for a family of frequency curves. Signal levels for small degradations (e.g. surface

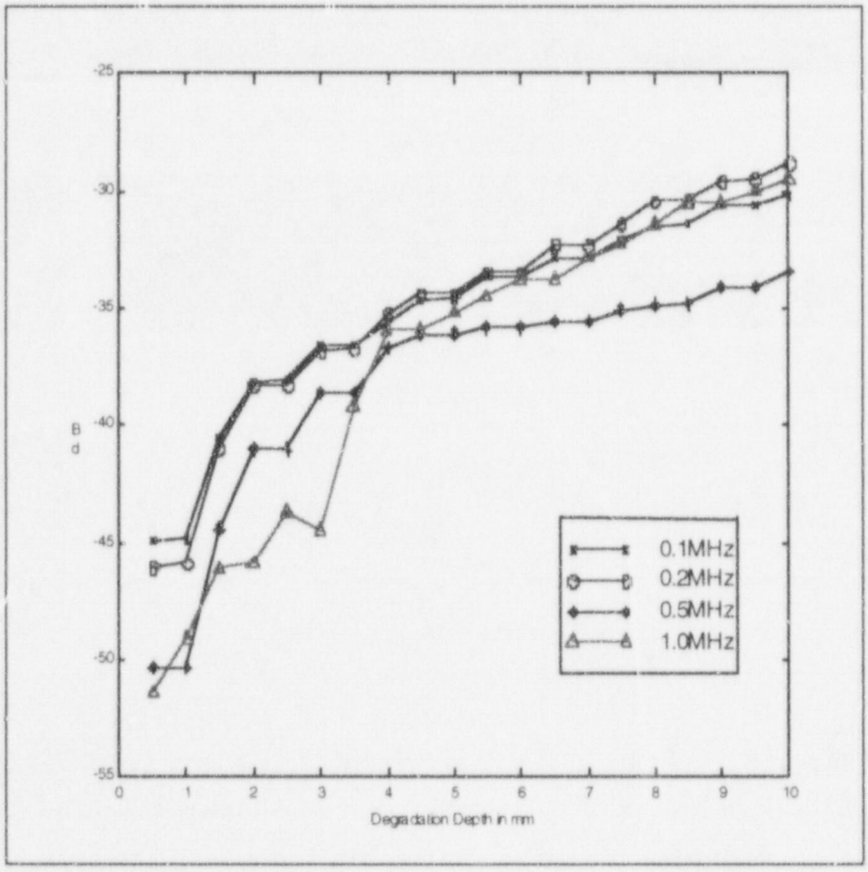

Fig. 3-8. Signal level from a degradation located 5 cm from the air/concrete interface vs degradation depth and frequency. Degradation on top and bottom surfaces. This shows that small degradations, below 2-mm-deep, reflect energy poorly. Thus, surface imperfections such as scratches will not be detected. Degradations above 2-mm-deep give appreciable signal levels and are easily detectable. The function of signal level with degradation depth is weak, but measurable.

scratches), below 1 mm are small, then, the curves all have a distinct rise at 2 mm. This is favorable news for a practical system. It says that such a system will be able to distinguish between small "surface imperfections" in the 0.5 to 1 mm range and degradations of a serious nature in the 2 to 10 mm range. The dependence over the 4 to 10 mm range is small, only about 10 dB, which implies that careful calibration will have to be done to determine degradation depth accurately. These results are for the sharp-sided notch. Other research [1] suggests that the pitting and shape of the degradation can have a significant effect on the backscatter level. This simulation thus indicates a "best case" backscatter scenario.

The shape of the curves in Fig. 3-8 are pleasing from an analytic standpoint. They are suggestive of classical scattering curves, which transition from low to high levels based on the scatterer size and frequency. In the field of sonar, it is well known that the directivity of scatter is tied to what is known as the Rayleigh parameter. The Rayleigh parameter, P, relates scatter directivity to wavelength and roughness height via:

$$P = 2k\sigma\cos(90-\alpha),$$

where $k = 2\pi/\lambda$ is wavenumber, λ is the wavelength, σ is the RMS displacement of the roughness, and α is the grazing angle. This is illustrated in Fig. 3-9. Intuitively, if the interrogating wavelength is large compared to the surface roughness, the wave tends to scatter mostly into the forward direction at the same angle. Thus, little energy is backscattered. If the interrogating wavelength is smaller than the surface roughness, the wave tends to scatter uniformly into all directions. Thus, significant energy is sent in the back direction. For the first mode in 25-mm-thick steel at 100 kHz, P = 243 σ, where at 200 kHz, P = 248 σ. This implies that for significant scatter we expect $\sigma > 4$mm, which is what our curves tell us.

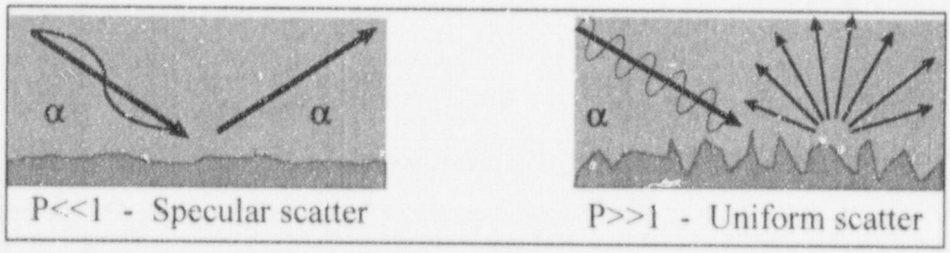

Fig. 3-9. Illustration of Rayleigh parameter, *P*. Smooth surfaces with respect to the ensonifying wave scatter energy forward while rough surfaces with respect to the ensonifying wave scatter energy in all directions.

For comparison, the field for a one-sided degradation was also computed. The model of Fig. 3-5 was run for frequencies of 0.1, 0.2, 0.5 and 1 MHz for a one-sided degradation whose depth ranged from 0.5 to 10 mm, incremented by 0.5 mm. Figure 3-10 shows a plot of signal level in dB versus degradation depth in millimeters for a family of frequencies. The degradation is located on the top surface, 5 cm to the right of the interface. Note that the levels compared to Fig. 3-8 are generally 3 dB lower, as would be expected for what is now half as much scatter.

Similar results are expected for a single-sided scatterer located on the bottom surface. Variation in the curves comes from the modal character of the field interacting with the exact location of the scatterer.

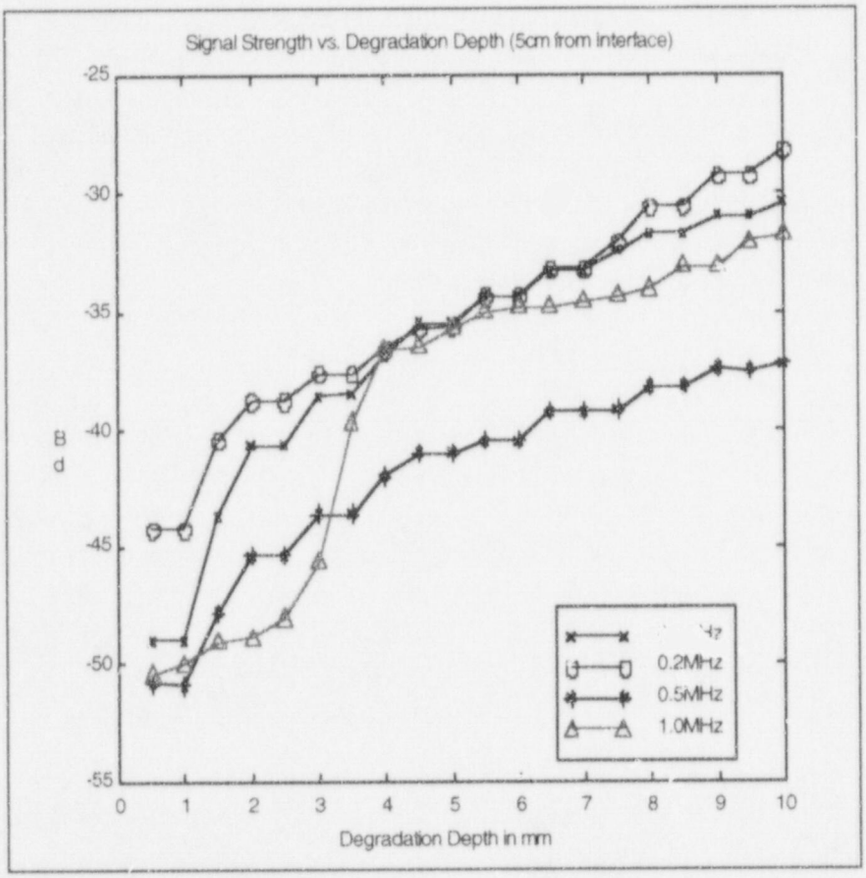

Fig. 3-10 Signal level from a degradation located 5 cm from the air/concrete interface vs degradation depth and frequency. Degradation on top surface only. This shows that small degradations, below 2-mm-deep, reflect energy poorly. Thus, surface imperfections such as scratches will not be detected. Degradations above 2-mm-deep give appreciable signal levels and are easily detectable. The function of signal level with degradation depth is weak, but measurable. This is similar to the results for two-sided degradations. Levels are generically 3 dB lower which is expected since the strength of the scattering notch has been reduced by half.

3.4.4 Penetration Study

In light of the air/concrete comparison between Fig. 3-6 and Fig. 3-7, it was felt that the location of the degradation from the interface would be a significant parameter in the problem. This would determine how much concrete a practical system could effectively penetrate. In order to determine the dependence of the field on this penetration depth, the model of Fig. 3-5 was run parametrically. Frequencies of 0.1, 0.2, 0.5 and 1 MHz were run for a two-sided, 4-mm-deep degradation located at 5, 10, 15 and 20 cm from the interface. Figure 3-11 shows a plot of signal level in dB versus penetration depth in centimeters for a family of frequency curves.

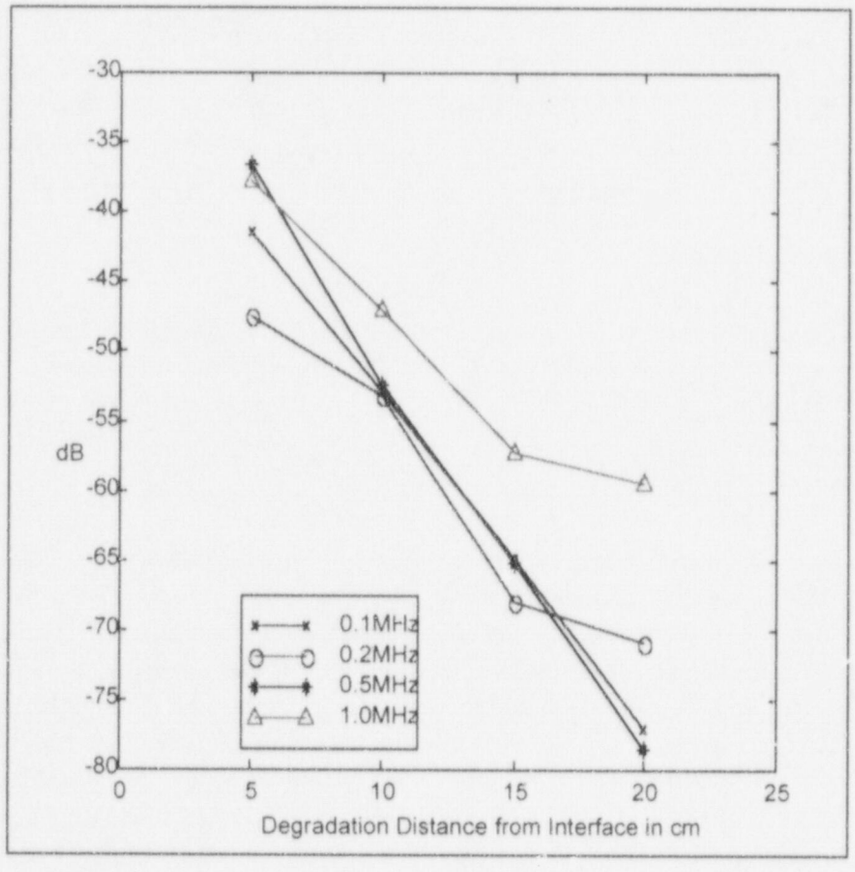

Fig. 3-11. Signal level from a 4-mm-deep degradation vs distance from interface and frequency. This figure shows that the presence of the concrete has a very large effect on the signal level. The concrete adds 3 - 4 dB of loss per centimeter penetrated. This will severely limit the penetration capability of any practical system to less than 30 cm below the interface.

The curves show a very high attenuation of the received signal with distance. Variation in the curves comes from the modal character of the field interacting with the exact location of the scatterer. The concrete adds 3 - 4 dB of two-way loss per centimeter of concrete penetrated. This will severely limit the penetration capability of any practical system. Since this dependence is much stronger than that seen with degradation thickness, it may limit a system's ability to effectively map degradation depths versus range. For example, with a range resolution of 0.5 cm, which is typical for these sensors, the signal will attenuate by 1.5 to 2 dB via leakage into the concrete. This imposes a degradation error level of about 2 - 3 mm given the variations shown in Fig. 3-10.

3.4.5 Source Angle Study

Sensor wedges come in a variety of angles to excite shear waves in steel. In order to determine the dependence of the field on source angle, the model of Fig. 3-5 was run parametrically. Frequencies of 0.1, 0.2, 0.5 and 1 MHz were run for a two-sided, 4-mm-deep degradation located 5 cm from the interface for wedge angles of 30, 45, 60 and 70 degrees (angle of shear wave in steel). Also, a wedge meant to excite surface waves was modeled and this is presented in Figure 3-12, which shows a plot of signal level in dB source angle for a family of frequency curves, as the 90 degree data point.

There is a maximum of 5 dB variation over angle and frequency for this degradation. It is believed that the modal structure in the steel at these frequencies is sufficiently rich and the beamwidths of the sensors are sufficiently wide that the input source angle is a minor effect.

3.4.6 Conclusions

For the embedded steel containment scenario, significant (2mm) degradations below the air/concrete interface give reasonable intrinsic backscatter level, -15 dB. These backscatter levels are 10-15 dB above the expected noise level due to "surface imperfections." The dependence of degradation depth is small, but measurable, being only 10 dB for degradation depths representing 10 to 80% of the section thickness. The embedding concrete introduces large losses, 3 - 4 dB two-way loss per cm of concrete. This will limit penetration capability. The range of depths that can be interrogated will depend on the capabilities of the transducer used. Calibration of such a system will be somewhat difficult because of this high loss. For example, the signal return from a 4-mm-deep degradation 7 cm away is equivalent to the signal return from a 8-mm-deep degradation 5 cm away. This problem can be mitigated with the use of time gating implemented in the processing software. Backscatter strength is not very sensitive to frequency or angle of the transducer (<5dB) for the sharp-edge degradations examined here. This may not be true for tapered degradations, higher losses should be expected. The numbers provided here assume a unit stress input, 0 dB. The output of currently available sensors is unknown. Receivers may or may not be able to pick up the returns from degradations and a test of a physically similar scenario with currently available sensors is required to determine if the observed transmission loss is tolerable. On the whole, the proposed approach appears feasible for the embedded containment scenario, provided transducer input power and sensitivity levels are sufficient.

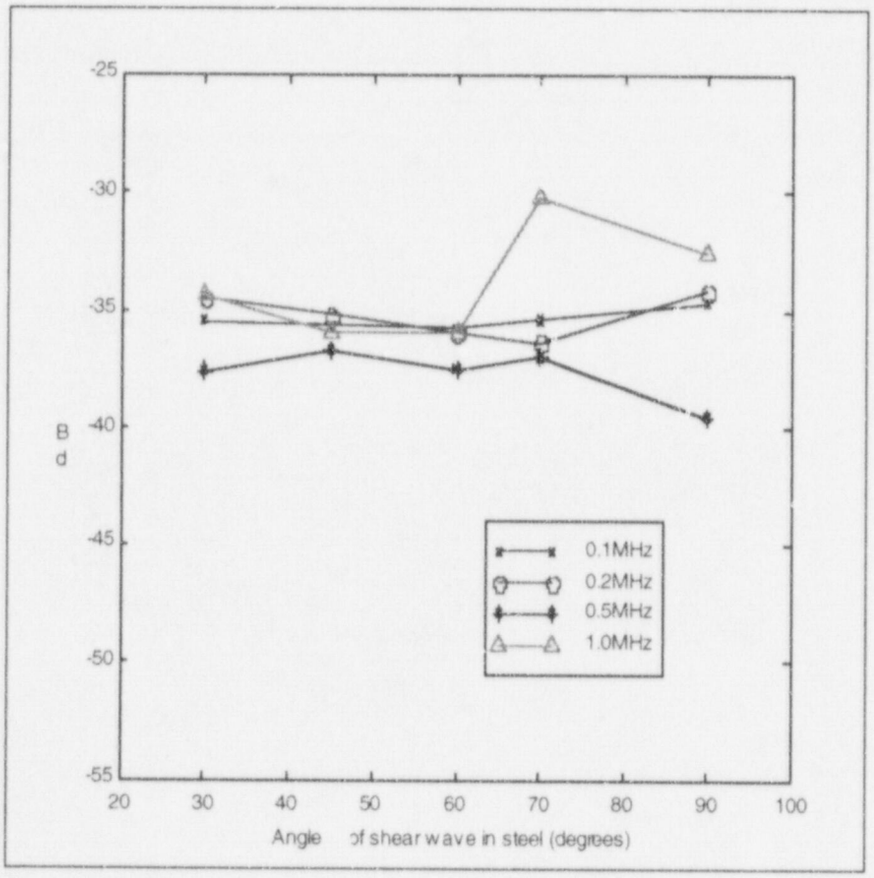

Fig. 3-12. Signal level from a 4-mm-deep degradation 5 cm from interface vs shear angle in steel. The signal level is fairly insensitive to the angle of sensor used. The beamwidths of these sensors are sufficiently wide to allow energy injection into the steel layer regardless of the angle used.

3.5 Range-Dependent OASES Studies on Steel-lined Concrete Containment

3.5.1 Scenario

The two-dimensional numerical model for the embedded steel-lined concrete containment scenario is shown in Fig. 3-13. The scenario is similar to the steel containment scenario, except the steel layer is now 6-mm-thick and there is concrete backing the entire steel layer. Concrete containments are generally on the order of 1 to 1.5 m thick. They are lined with a 6-mm-thick steel layer. Since the purpose here is to detect degradation in the liner, the field should be restricted to the steel layer. For this reason and since the liner is much thinner than the concrete, the concrete containment was modeled as a pure halfspace.

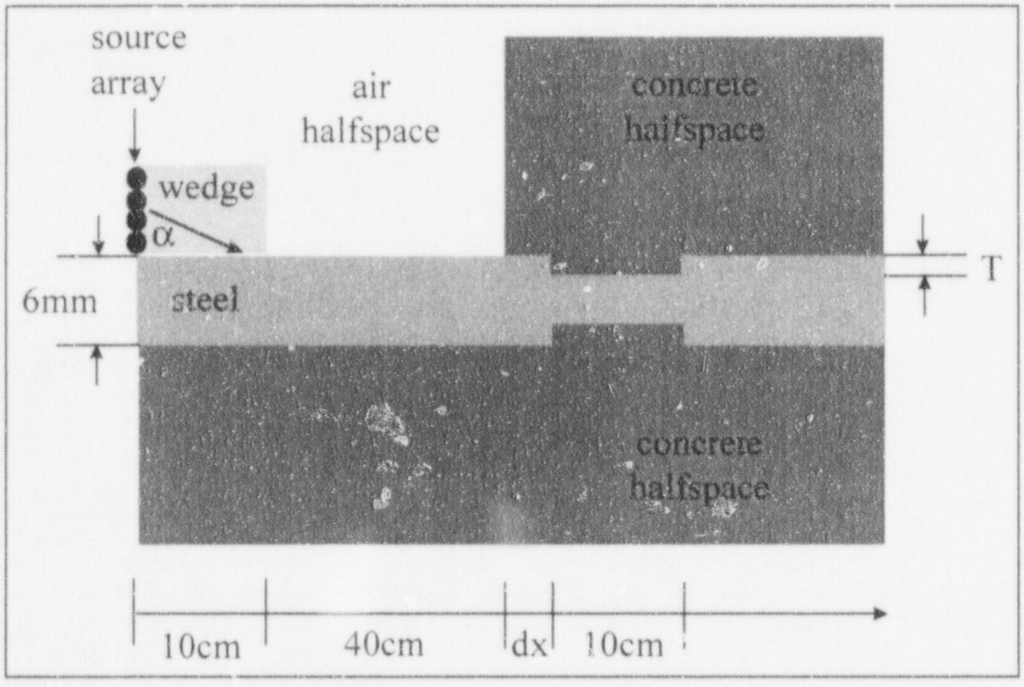

Fig. 3-13. Simulation scenario for steel-lined concrete containment. 6-mm-thick steel layer backed by a concrete halfspace below. Top is bounded by a concrete halfspace on the right and by an air halfspace on the left. Degradation is modeled by a two-sided 10-cm notch cut from the steel layer and filled with concrete. The thickness of the layer, T, and its distance from the interface, dx, are parameters of the simulation.

3.5.2 Results

Figure 3-14 shows normal stress in dB as a function of depth and range for the forward- and back-propagating fields resulting from a 0.5 MHz, 25-mm-long source array coupled with a wedge to excite a 45-degree shear wave in the steel. There is a 2-mm-deep, two-sided

degradation located 5 cm from the air/concrete interface. The dynamic range of these plots has been extended to accommodate the higher losses due to the additional concrete.

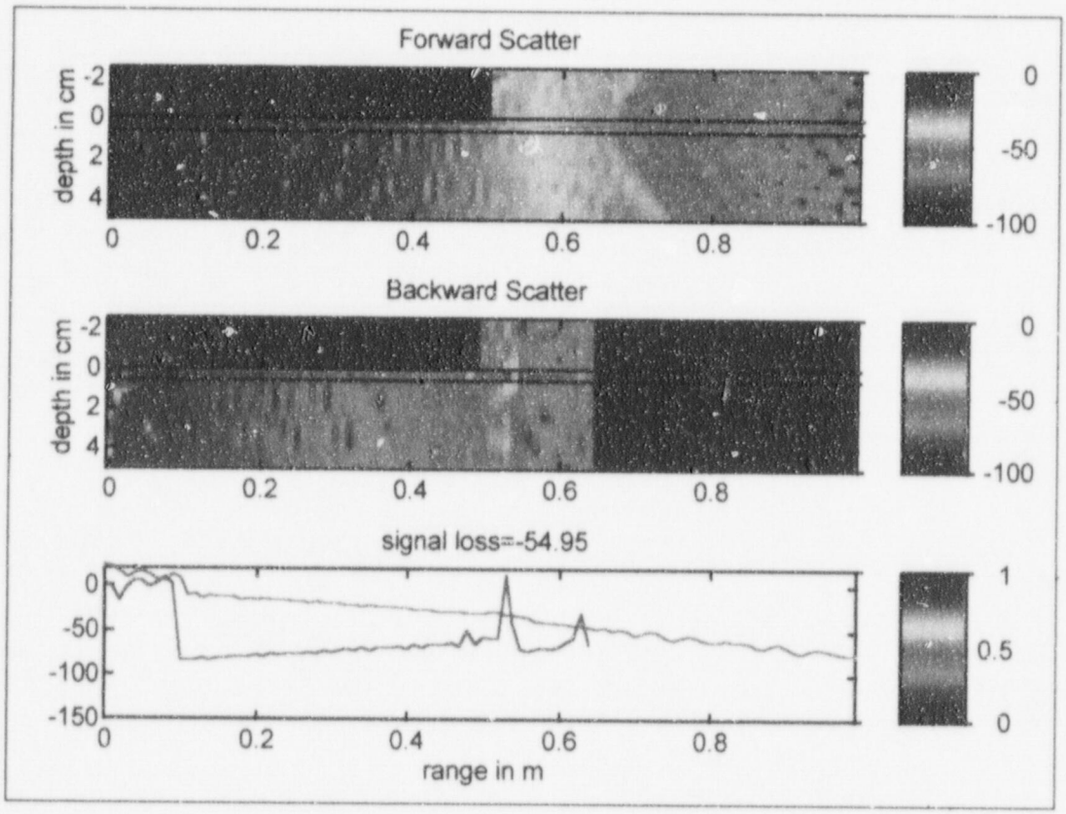

Fig. 3-14. Model of an embedded steel-lined concrete containment. The source is a 0.5 MHz, 25-mm-long array which excites a 45-degree shear wave in steel, located at 0 m range above top surface. The degradation is modeled as a two-sided, 2-mm-deep notch, 10–cm long, starting at 0.55 m. The top plot represents the forward-propagating energy as a function of distance and depth, and the middle plot represents the backward-propagating energy. Colors represent normal stress in dB. The bottom plot shows the forward-propagating amplitude measured at the top surface in blue and the backward-propagating amplitude in red. Signal loss is an average value of the difference of these two over the range 10 to 50 cm. Note that much of the forward energy is injected through the steel plate directly into the concrete and lost. Returned signal levels are very low, owing to the high loss of energy to the concrete. Levels are 40 dB (factor of 100) lower than the comparable number for the steel containment scenario.

Note that the source is injecting energy through the plate into the concrete directly. This is energy that is no longer forced to propagate in the plate and is now unavailable to interrogate the degradation in the steel containment scenario. This lost energy will limit the ability of a practical system to excite waves in the liner. Though not modeled here, the energy injected into the concrete directly causes an additional problem. If there are scatterers in the concrete, in the form of voids or reinforcing steel bars local to the plate, they will tend to scatter energy back up to the plate and may cause interference with the desired measurements. While this is also a concern in the steel containment scenario, excitation of the scatterers there is from a secondary mechanism (i.e., from the plate leakage). It is more problematic here due to the direct excitation of the concrete.

Of course the primary difficulty here is the enormous loss of energy from the plate to the concrete, due to the thinness of the steel layer and the greater extent of the concrete. The signal level here is SL = -80 dB, which is four orders of magnitude down from the levels seen in the steel containment scenario. The detection and penetration capabilities of a practical system will be extremely limited in this case.

3.5.3 Degradation Depth Study

In order to determine the dependence of the field on frequency and depth of the degradation, the model of Fig. 3-13 was run parametrically. Frequencies of 0.1, 0.2, 0.5 and 1 MHz were run for two-sided degradation depths ranging from 0.5 to 3 mm, incremented by 0.5 mm. Figure 3-15 shows a plot of signal level in dB versus degradation depth in millimeters for a family of frequency curves. As discussed above, the signal level is very small for this scenario, due to the high loss to the concrete and thinness of the steel layer. The scattering curves for the two higher frequency cases, 0.5 and 1.0 MHz, show a classical scattering curve, this time with the knee of the curve at 1 mm as should be expected for a much thinner steel layer. The lower frequencies show a much higher returned signal level. It was thought at first that these higher levels were beneficial. However, these curves do not have a classical scattering characteristic.

On further investigation, see Fig. 3-16, it was found that these low frequency sources are not able to couple into the modes of the plate. They are exciting the entire layered system in a piston-like fashion. While this is possible numerically, a practical sensor would not have the power to move the concrete in this fashion. Thus, this is an unrealistic scenario from the practical standpoint.

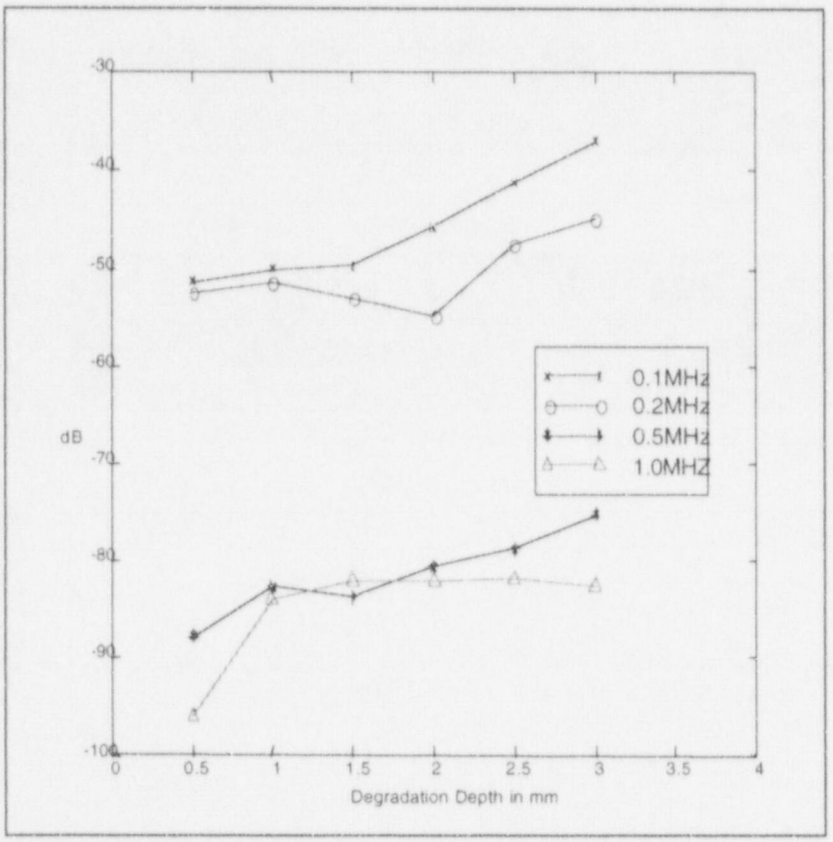

Fig. 3-15. Signal level from a degradation located 5 cm from the interface vs degradation depth and frequency. This shows that low frequencies have a high level of return versus high frequencies. Unfortunately, this result has been shown to be unphysical. The function of signal level with degradation depth is weak, but shows no discrimination against small degradations. Thus, surface imperfections (i.e., scratches) could be incorrectly identified as degradations by a practical system. The high frequency results show unacceptably high loss to the concrete, which brings the feasibility of a practical system for this scenario into question.

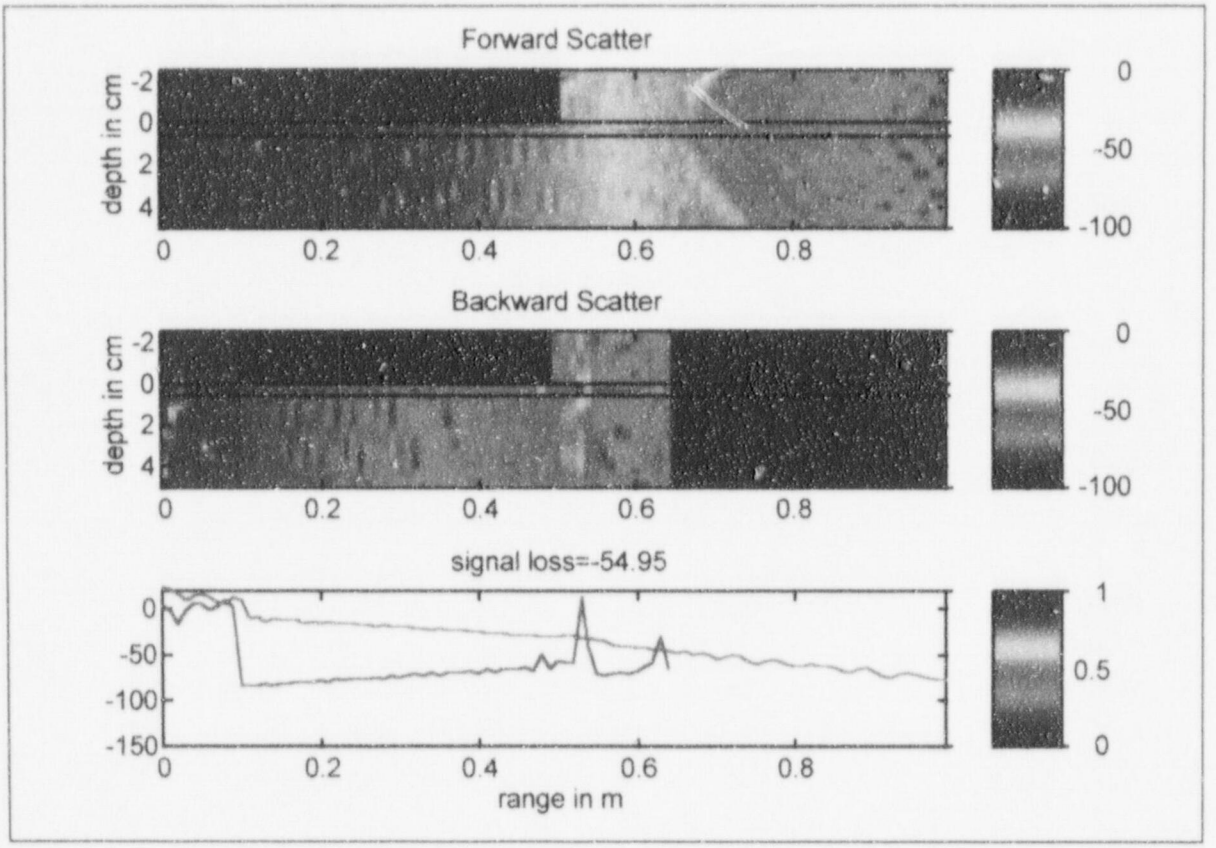

Fig. 3-16. Model of an embedded steel-lined concrete containment. The source is a 0.2 MHz, 25-mm-long array that excites a 45-degree shear wave in steel, located at 0 m range above top surface. The degradation is modeled as a two-sided, 2-mm-deep notch, 10-cm long, starting at 0.55 m. The top plot represents the forward-propagating energy as a function of distance and depth, and the middle plot represents the backward-propagating energy. Colors represent normal stress in dB. The bottom plot shows the forward-propagating amplitude measured at the top surface in blue and the backward-propagating amplitude in red. Signal loss is an average value of the difference of these two over the range 10 to 50 cm. This model depicts the unphysical nature of the low frequency results. The entire concrete halfspace is being excited by the source in a piston like fashion. No practical source would produce enough energy to do this. Even if it could, scatterers present in the concrete, such as rebar, would overwhelm the return from the degradation in the steel plate.

3.5.4 Penetration Study

Although it is highly unlikely that any practical sensor system could overcome such high losses associated with the steel-lined concrete containment scenario, for completeness, a penetration study was conducted for this case as well. In order to determine the dependence of the field on penetration depth, the model of Fig. 3-13 was run parametrically. Frequencies of 0.1, 0.2, 0.5 and 1 MHz were run for a two-sided, 2-mm-deep degradation located a 5, 10, 15 and 20 cm from the interface. Figure 3-17 shows a plot of signal level in dB versus penetration depth in centimeters for a family of frequency curves.

Results show again 3-4 dB of two-way signal loss per centimeter of concrete penetrated. The added loss in this case seems to come from the additional concrete on the bottom of the steel layer to the left of the interface. Losses on the order of 100-140 dB mean that the penetration and detection capability of a practical system are extremely limited. For this reason it is unlikely that high frequency imaging technology will be applicable to this scenario.

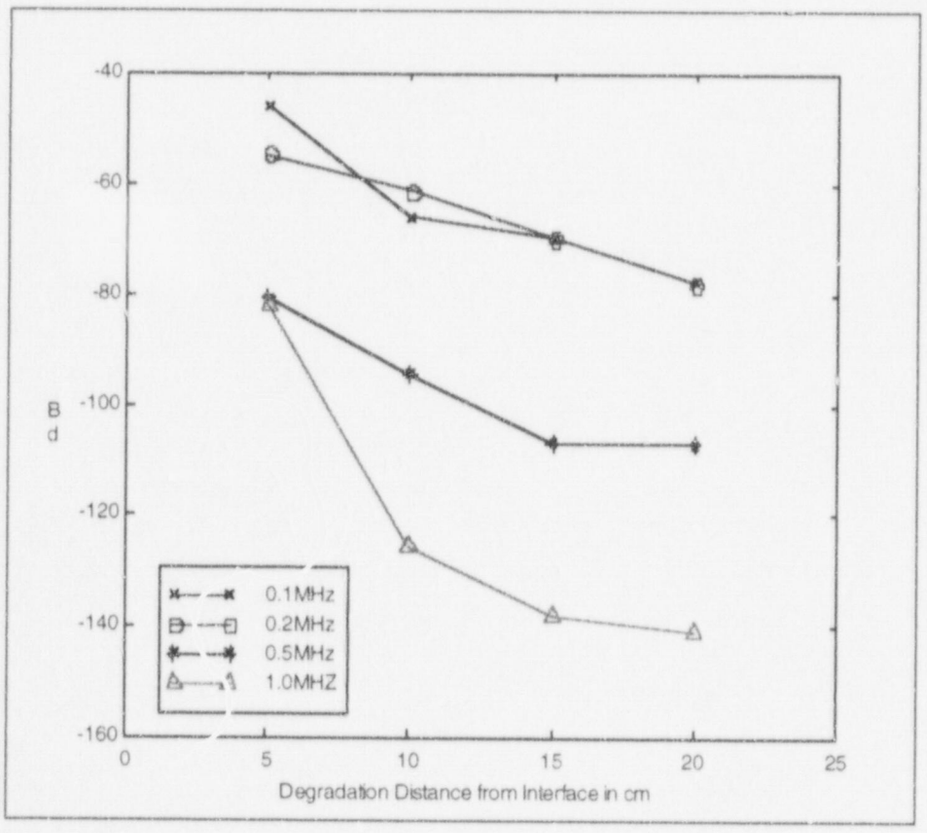

Fig. 3-17. Signal level from a 2-mm-deep degradation vs distance from interface and frequency. The signal levels for the high frequency curves are extremely small due to the high loss of energy into the concrete, even for large degradations near the surface. For this reason, it is highly unlikely that acoustic imaging technology can be applied to the steel-lined concrete containment scenario.

3.5.5 Conclusions

For the embedded steel-lined concrete containment, the thin steel layer and additional concrete backing contribute to give unacceptably high loss to concrete, on the order of 100 dB, for a small degradation close to the interface. Frequencies that do not excite plate modes (i.e., below 500 kHz) tend to drive the entire concrete-steel system and will cause high power loss at the source and likely cause interference from voids, reinforcing bars, and aggregate in the concrete. Higher frequency sources tend to drive energy through the plate and thus will be highly inefficient. Due to the high loss to the additional concrete, they will have a severely limited detection capability. It is highly unlikely that acoustic imaging technology can be applied to this scenario.

4. SYSTEM REQUIREMENTS – THREE-DIMENSIONAL ISSUES

The physics of wave propagation within the containment wall were determined primarily by the two-dimensional layered system shown on the left side of Fig. 1-1. Now that this process is understood, the restrictions imposed by important parameters of the two-dimensional scenario and the sensors themselves permit exploration of specific three-dimensional scenarios like the one shown in the right side of the same figure. The goal is to design an array of sensors that can scan the surface of the containment to localize and map thickness degradations. The area of interest is the region up to 30 cm below the air/concrete interface around the entire containment. This chapter describes the important parameters of array design. It will be shown that current sensor technology does not allow array-based designs. Thus, the application of these sensors will be limited to spot inspections where degradation is already suspected rather than wide-area surveys for preliminary detection of degradation.

4.1 Array Approach for Localization and Mapping

Localization and mapping are similar operations from the point of view of a sensor system. Generally, a sensor system searches an area or volume by scanning in two or three dimensions. The search can be *active*, where the sensor sends out pulses of energy and listens for returns, or *passive*, where the sensor just listens for energy from an active source. The system under consideration here is an active system, since there are no active sources in our scenario. For an active system, one must be able to put energy into the medium and get enough signal bounced back from the target to be measurable at the receiver. The search area or volume is divided up into *bins* in some coordinate system – rectangular, cylindrical, or spherical. The result of the sensor sweep is recorded for each bin. If the record is a "target/no target" decision, this is known as localization. The information is primarily location of a target. If the record is a received level, either raw data or data interpreted via some transform, this is known as mapping. The problem at hand is a mapping problem, as the desired output is a spatial map of the degree of degradation over the entire surface of the containment.

Array processing is used to do either localization or mapping. Localization is a bit easier to describe. From there, mapping is a simple generalization. In order to localize a point scatterer, several directional views of it must be obtained and correlated. A classical way to do this in two dimensions is with an array of sensors using a "range-bearing" type of algorithm [12]. This is illustrated in Fig. 4-1.

Typically, a line array of N individual, omni-directional sensors is used in a coherent fashion. In a narrowband frequency sense, the sensors are electronically phased to transmit and receive a tight angular beam of propagating energy. As shown in the left hand side of Fig. 4-1, this beam can be steered in a particular direction, θ. By sweeping the beam over this angle and identifying which angle gives the strongest return, the bearing of the target relative to the array can be found.

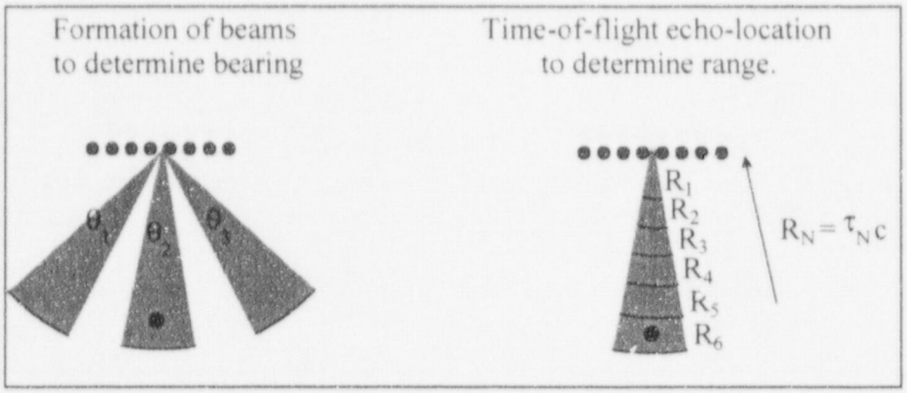

Fig. 4-1. Illustration of localization via beam steering for bearing determination and range gating for range determination.

Once bearing is known, the range is found by using time-of-flight information. The range of the target is given by multiplying the two-way travel time, 2τ, by half the soundspeed of the medium, $c/2$. This range information along with the bearing information locate the target uniquely in the cylindrical coordinate space (although a line array does have an up-down ambiguity). The accuracy of this localization is dictated by the *resolution* of the array in the angular direction and the *bandwidth* of the pulse in the range direction. These constraints give the minimum bin size in the two directions.

Figure 4-2 is a simple illustration of the important parameters that govern the *resolution* of line arrays. In order to avoid spatial aliasing of the array, the elements must have a spacing, dx, smaller than $\lambda/2$, where λ is the wavelength of the signal ($\lambda=c/f$), c is the sound speed of the material, and f is the frequency of the signal. This is similar to the Nyquist condition of signal processing and must be met to prevent bearing ambiguity. In the far-field, the beam pattern of the array is a sine function whose main lobe width is dictated by the length of the array, L. The angular resolution, θ_{3dB}, of the array in radians is simply the wavelength, λ, divided by the length

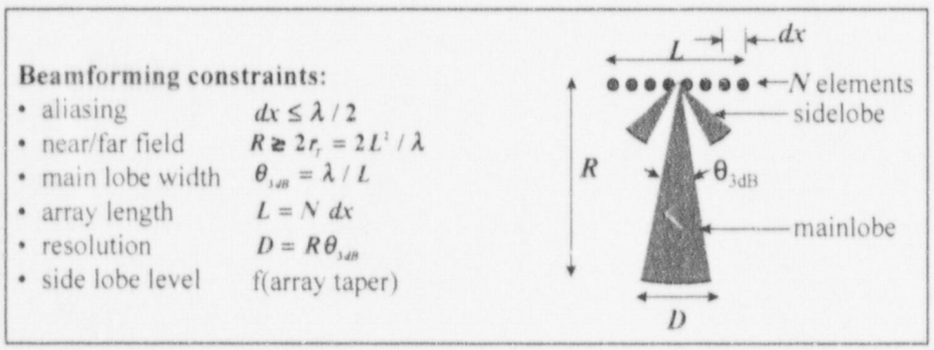

Fig. 4-2. Illustration of beamforming parameters and their effect on beam shape.

of the array, L. The resolution, D, at a particular range, R, is this angular resolution multiplied by that range. This is only true in the far-field of the array which starts at a range equal to $2r_T = 2L^2/\lambda$. The strength of the array sidelobes is a function of the amplitude taper applied across the array. For a Hamming taper, a target in the sidelobe will have a level more than 40 dB below the level of a target in the mainlobe. The range bin size is proportional to the duration of the pulse sent out by the source as shown in Fig. 4-1. A good estimate of this pulse duration is: $\tau = 1/Bw$, where Bw is the bandwidth of the signal.

4.2 Localization and Mapping with Ultrasonic Sensors

The characteristics of typical ultrasonic sensors are listed in Table 2-1. From these characteristics bin sizes can be calculated. The range bin width is computed from the bandwidth of the sensor. With a $Q = \Delta f/f_C = 0.6$, a 1 MHz sensor has a $\tau = 1.7$ μs or $\Delta R = 5$ mm. Thus, the range bin size is 0.5 cm. The total range of interest is on the order of 30 cm, which is equal to about 60 bins. This is not a very taxing burden for a system to measure and calculate. Since one would like to localize down to about 3 cm in this application, a 0.5 cm wave bin size more than meets the criterion and is a good practical range resolution.

The angular resolution is more of a problem with available sensors. A typical sensor is in the form of a piston which is not small compared to a wavelength. This is *not* an omni-directional source, as is required for the formation of an array. To understand the high directionality of this sensor, one can model it as a dense array of finite length L, phased coherently in one direction. At 1 MHz, a 25-mm shear sensor *itself* has a main lobe width of only $\theta_{3dB} = 7^\circ$. To understand the severity of this limitation, note that at 25 cm away from sensor, the sensor interrogates a spot only D = 3 cm wide. These ultrasonic sensors cannot be used together in a scanning array. The individual sensor beam pattern would make looking in any direction other than the intrinsic sensor direction impossible. Thus, the current sensor technology can only be used in spot detection and mapping scenarios. If there was suspected degradation in an area of the containment, the sensor could be physically moved along at 3 to 5–cm intervals to sweep out a small area. This is an intensive manual process which would be warranted if degradation was suspected, but prohibitive for a wide-area scan.

4.3 Scannable Sensors

It would not be practical to interrogate a large area with currently available sensors. A scannable sensor technology, like those used for medical ultrasound, should be investigated. These sensors are manufactured by bonding many signal wires to a solid piezoelectric block on a substrate and then cutting the piezo into individual sensors, leaving a line array of N sensors in the substrate. This is shown in Fig. 4-3. For example, at 1 MHz, the spacing on this array would have to be on the order of 1.5 mm to avoid aliasing and 25.4 mm in total length for an angular resolution of $\theta_{3dB} = 7^\circ$. This would be a 17-element array, which would be very reasonable to drive electronically in terms of cost and complexity. The finite size of the individual sensors

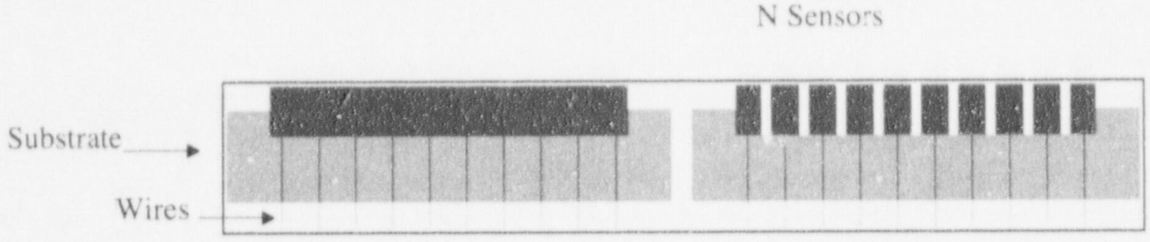

Fig. 4-3. Sensor array cut from a single sensor block. Left side shows initial bonding of piezo material to wires and substrate. Right side shows array cut into individual elements prior to potting.

would allow a total scan sector width of 120°. This would give about 18 angular bins. Experiments with the wedge material would have to be made to insure that the directionality of the sensor would not interfere with the coupling characteristics of the wedge and vice versa.

Given the fixed scan sector size of 120°, the maximum penetration ability of the sensor and the required depth of coverage, will limit the array offset, as seen in Fig. 4-4. This is the separation between scanning stations (i.e., manual positioning of the array along the containment). The scan cones must overlap, as shown in the figure, for complete coverage. It is anticipated for the current estimates of these parameters that the array offset will be on the order of 1.5 m. This means about 75 stations around a 36-m-diameter containment, which is time consuming but reasonable for a wide area search.

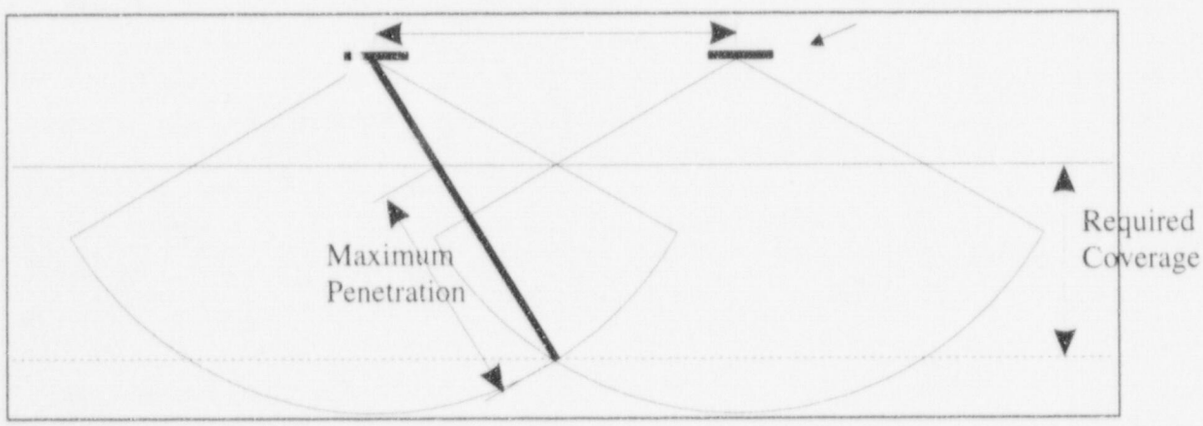

Fig. 4-4. Array spacing and beam overlap for a scannable array system. The maximum penetration is dictated by the propagation physics. This and the required coverage limit the array offset to 1.5 m for complete interrogation of the required area.

5. CONCLUSIONS AND RECOMMENDATIONS

5.1 Conclusions

Due to the embedding concrete, lower portions of steel and steel-lined concrete containments of U.S. nuclear power plants cannot be inspected effectively by conventional UT methods. Few alternatives, such as expensive and destructive chipping of concrete, exist. As an alternative, this report presents results of a numerical feasibility study that was conducted to investigate the use of high-frequency acoustic imaging techniques to map degradation of the inaccessible areas of the containment.

The characteristics of current sensor technology are inadequately specified and calibrated to determine their applicability to the above. The a*bsolute* vibration levels generated by sources in the containment scenario cannot be accurately predicted; only relative measures of transmission loss due to normalized input levels can be assessed. However, the frequency ranges, sizes, and orientations of available sensors can be used in the numerical models. Previous efforts to detect surface degradations with primitive high-frequency imaging equipment have met with moderate success, which indicates that the basic idea has merit.

The numerical model, Range-Independent OASES, was used to represent the steel containment scenario but failed to model correctly the surface degradation. However, the Range- Dependent version of the code successfully modeled this scenario using a discrete notch approach, as well as the steel-lined concrete containment scenario. The fields that would be seen by currently available sensors were calculated analytically to assess the backscattered returns from a variety of thickness degradations. Results of this numerical modeling work are as follows:

- Analytical simulation suggests that for the embedded steel containment scenario: Significant (2 mm) degradations below the air/concrete interface give a reasonable intrinsic backscatter level, -15 dB, which is 10-15 dB above the expected noise level due to "surface imperfections." The dependence of degradation depth is small, only 10 dB over 10%-80% of containment thickness, but measurable. The embedding concrete introduces large losses, 3-4 dB two-way loss per cm of concrete and will limit penetration capability. Backscatter strength is not very sensitive to frequency or angle of the transducer (< 5 dB) for the sharp-edge degradations examined here. These results indicate that it is probable that acoustic imaging technology can be applied to this scenario.

- Analytical simulation suggests that for the embedded steel-lined concrete containment: The thin steel layer and additional concrete backing contribute to give unacceptably high loss to concrete, ~100dB, for a small degradation close to the interface. Due to this loss, it is highly unlikely that acoustic imaging technology can be applied to this scenario.

Finally, array configurations for this application were discussed. Currently available sensors cannot be used in array configurations, due to their intrinsic narrow beampattern, which does not allow steering. This limits these sensors to spot detection and mapping scenarios,

where degradation is already suspected. For wide-area surveys, scannable sensors will have to be developed in a future effort. This technology will widen the scope of application to practical wide-area surveys.

5.2 Recommendations

This work provides basic information on the expected backscattered signal from numerically simulated degradations due to a unit stress input. It remains to be seen if current sensor technology can input sufficient power into the system to obtain return levels within the dynamic range of currently available receiver systems. A controlled experimental testing program to calibrate sensor levels against degradations is essential to determine these return levels. It is hoped that this knowledge will allow us to determine if these systems can be specified for use in regular containment inspection programs.

A test plan that encompasses numerical simulations, laboratory calibration of current sensor technology, and field testing to collect example containment data is as follows:

- Conduct a set of numerical studies via RD-OASES to quantify the effect of studs connected to the embedded steel and rebar embedded in concrete on the returned levels from degradations. Possible scenarios are shown in Fig. 5-1.

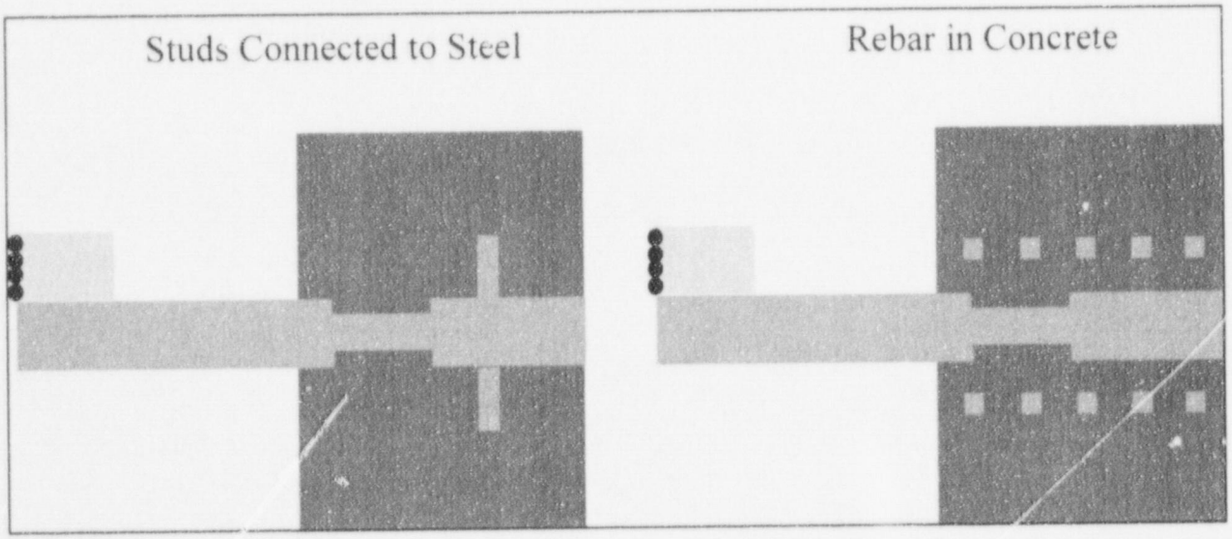

Fig. 5-1. RD-OASES simulation scenario for additional scatterers. Left side shows a model that includes anchor rods welded to the steel layer. Right side shows a model which includes reinforcing bar in concrete.

- Perform a test series in the laboratory to calibrate existing sensors. This would involve procurement of a set of typical sensors and a pulser/receiver unit to drive them. The output power of the sensors would be measured along with vibrational levels backscattered from a set of test blocks with sample simulated degradations.

- Using results of the laboratory test series, estimates made by RD-OASES could be refined to account for input power and any additional phenomenon such as loss to out-of-plane scattering.

- Once the sensor systems have been understood, a major series of laboratory or field tests could be performed. Either available containment test sections or actual containments at sites that are decommissioned or in the process of being decommissioned could be used for the testing. Data collected would be used to assess sensor performance under representative conditions.

- This experimental data would be processed and compared to the RD-OASES models for model refinement and identification of any phenomenon not understood to that point.

- Finally, a total assessment of the method, available technology, performance, and recommendations could be assimilated. It would be appropriate here to specify and cost the development of a scannable sensor array.

6. REFERENCES

[1] Pocock, D.C. et al., Long-term Performance of Structures Comprising Nuclear Power Plants, Commission of the European Communities, CD-NA-12758-EN-C, 1990.

[2] Viktorov, I.A., Rayleigh and Lamb Waves: Physical Theory and Applications, Plenum Press, NY, 1967.

[3] Simaan, M. et al., "Nondestructive detection of Flaws in Material Using Transducer Arrays," Nondestructive Evaluation, Vol 6, No 1, p. 47-55, 1987.

[4] Coffey, J., Chapman, R.K. "Application of Elastic Scattering Theory for Smooth Flat Cracks to the Quantitative Prediction of Ultrasonic Defect Detection and Sizing.", Nucl. Energy, 1983, No5. Oct., 319-333.

[5] Budreck, D.E., "Ultrasonic Scattering From a Crack which Emanates from a Rivet Hole.", Quantitative Nondesstructive Evaluation Vol 12, 1993 pp 83-91.

[6] The online Journal of Nondestructive Testing & Ultrasonics, URL: www.ultrasonic.de

[7] Chimenti, D., "Guided Waves in the Presence of Rough Surfaces", Seminar at Boston University 10 Oct 1997. (Iowa State Center for Non-Destructive Evaluation).

[8] Schmidt, H., SAFARI: Seismo-Acoustic Fast-field Algorithm for Range Independent environments, User's Guide, SACLANT ASW Research Centre I-19100 La Spezia, Italy, May 1987.

[9] Schmidt, H., OASES User Guide and Reference Manual Version 2.1, MIT, 1997.

[10] OASES download URL: http://dipole.mit.edu:8001/arctic0/henrik/www/home.html

[11] Gere, J.M. and Timoshenko, S.P., Mechanics of Materials, PWS-Kent, Boston,1990.

[12] Johnson, D.H. and Dudgeon, D.E., Array Signal Processing, Prentice Hall, N.J. 1993.

NRC FORM 335 (2-89) NRCM 1102, 3201, 3202

U.S. NUCLEAR REGULATORY COMMISSION

BIBLIOGRAPHIC DATA SHEET

(See instructions on the reverse)

1. REPORT NUMBER (Assigned by NRC, Add Vol., Supp., Rev., and Addendum Numbers, if any.)

NUREG/CR-6614
ORNL/SUB/97-SX754V

2. TITLE AND SUBTITLE

Feasibility of High Frequency Acoustic Imaging for Inspection of Containments

3. DATE REPORT PUBLISHED

MONTH	YEAR
August	1998

4. FIN OR GRANT NUMBER

J6043

5. AUTHOR(S)

J.E. Bondaryk, C.N. Corrado, Oak Ridge National Laboratory
V. Godino, Engineering Technology Center

6. TYPE OF REPORT

Technical

7. PERIOD COVERED *(Inclusive Dates)*

8. PERFORMING ORGANIZATION - NAME AND ADDRESS *(If NRC, provide Division, Office or Region, U.S. Nuclear Regulatory Commission, and mailing address; if contractor, provide name and mailing address.)*

Oak Ridge National Laboratory
Operated by Lockheed Martin Energy Research Corporation
Oak Ridge, TN 37831

Subcontractor:
Engineering Technology Center (ETC)
240 Oral School Road, Suite 105
Mystic, CT 06355-1208

9. SPONSORING ORGANIZATION - NAME AND ADDRESS *(If NRC, type "Same as above", if contractor, provide NRC Division, Office or Region, U.S. Nuclear Regulatory Commission, and mailing address.)*

Division of Engineering Technology
Office of Nuclear Regulatory Research
U.S. Nuclear Regulatory Commission
Washington, DC 20555-0001

10. SUPPLEMENTARY NOTES

H.L. Graves III, NRC Project Manager

11. ABSTRACT *(200 words or less)*

This numerical feasibility study investigated the use of high-frequency bistatic acoustic imaging techniques for inspection of inaccessible portions of the metallic pressure boundary of nuclear power plant containments. High frequency vibrational sources were used to excite elastic waves in the steel. Waves that reflect and scatter from surface roughness caused by degradations (e.g., corrosion) are detected and used to identify and map the steel degradation. Variables in the study included frequency, flaw size, interrogation distance, and sensor incident angle. Results for portions of steel containments embedded in concrete indicate that the intrinsic backscatter from degradations representing thickness reductions from 10 to 80% the shell thickness are sufficient to permit detection. For the embedded steel liner of reinforced concrete containments, the thin steel layer and high signal losses to the concrete indicate that it is unlikely that acoustic imaging technology can be applied to this scenario. It is recommended that a controlled experimental program be conducted in which sensor levels are calibrated against degradations to determine if current sensor technology can input sufficient power into the system to provide return levels within the dynamic range of the receivers.

12. KEY WORDS/DESCRIPTORS *(List words or phrases that will assist researchers in locating the report.)*

acoustic imaging
containment
degradation
inspection
liner
nondestructive examination
numerical modeling
shear waves
ultrasonics

13. AVAILABILITY STATEMENT

unlimited

14. SECURITY CLASSIFICATION

(This Page)
unclassified

(This Report)
unclassified

15. NUMBER OF PAGES

16. PRICE

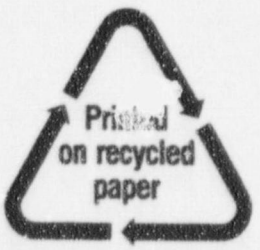

Federal Recycling Program

UNITED STATES
NUCLEAR REGULATORY COMMISSION
WASHINGTON, DC 20555-0001

OFFICIAL BUSINESS
PENALTY FOR PRIVATE USE, $300

FIRST CLASS MAIL
POSTAGE AND FFES PAID
USNRC
PERMIT NO. G-67

120555154486 1 1AN1RD1R9
US NRC-OCIO
DIV-INFORMATION MANAGEMENT
TPS-PDR-NUREG
2WFN-6E7
WASHINGTON DC 20555